Inhibitory interneurons distribute widely across the mouse thalamus and form ontogenetic spatial clusters

Polona Jager[1], Padraic Calpin[2], Xhuljana Durmishi[1], Tomomi Shimogori[3], Alessio Delogu[1]*

[1] Department of Basic and Clinical Neuroscience, Institute of Psychiatry, Psychology and Neuroscience, King's College London, London, UK

[2] Department of Physics and Astronomy, University College London, London, UK

[3] Center for Brain Science, RIKEN, Saitama, Japan

* Correspondence: alessio.delogu@kcl.ac.uk

Abstract

The proportion and distribution of local inhibitory neurons (interneurons) in the thalamus varies widely across mammals. This is reflected in the structure of thalamic local circuits, which is more complex in primates compared to smaller-brained mammals like rodents.

An increase in the number of thalamic interneurons could arise from addition of novel interneuron types or from elaboration of a plesiomorphic ontogenetic program, common to all mammals. The former has been proposed for the human brain, with migration of interneurons from the ventral telencephalon into higher order thalamus as one of its unique features (Letinic and Rakic, 2001).

Here, we identify a larger than expected complexity and distribution of interneurons across the mouse thalamus. All thalamic interneurons can be traced back to two developmental programs: one specified in the midbrain and the other in the forebrain. Interneurons migrate to functionally distinct thalamic nuclei, where the midbrain-derived cells populate the sensory thalamus, and forebrain-generated interneurons only the higher order regions. The latter interneuron type may be homologous to the one previously considered to be human-specific, while we also observe that markers for the midbrain-born class are abundantly expressed in the primate thalamus. These data therefore point to a shared ontogenetic organization of thalamic interneurons across mammals.

Introduction

The thalamus is a forebrain structure that develops from the diencephalic prosomere 2 (p2) (Puelles and Rubenstein, 2003; Shi et al., 2017; Wong et al., 2018) and is primarily composed of cortically projecting excitatory thalamocortical (TC) neurons, divided into more than 30 individual nuclei in mammals (Jones, 2007; Clascá, Rubio-Garrido and Jabaudon, 2012; Hunnicutt et al., 2014). The function of the thalamus has been historically described as relay of sensory information to the cortex (Hubel and Wiesel, 1962; van der Loos and Woolsey, 1973; Shatz, 1996; Sherman and Guillery, 2002; Cheong et al., 2013; Piscopo et

al., 2013; Zeater et al., 2015). Taking into account the diversity of input and output features of thalamocortical circuits (Herkenham, 1980; Guillery, 1995; Rubio-Garrido et al., 2009; Clascá et al., 2012; Sherman, 2016), more recent work has shown that the thalamus is also critically involved in cognitive processes allowing for behavioural flexibility (Saalmann and Kastner, 2011; Groh et al., 2014; Ling, Pratte and Tong, 2015; Sherman, 2016; Bolkan et al., 2017; Guo et al., 2017; Schmitt et al., 2017; Rikhye, Gilra and Halassa, 2018; Rikhye, Wimmer and Halassa, 2018).

In contrast to cortical networks, excitatory neurons in the thalamus do not connect with each other (Jones, 2007; Bickford et al., 2008; Hirsch et al., 2015; Rikhye et al., 2018b). Instead, local connections and computations within thalamocortical circuits are dominated by the resident inhibitory, GABA-releasing neurons (interneurons) (Pasik, Pasik and Hamori, 1976; Montero, 1987; Sherman, 2004; Hirsch et al., 2015).

Interneuron numbers and distribution vary widely across species, suggesting that they are critically involved in the evolution of thalamocortical structure and function (Arcelli et al., 1997; Letinic and Rakic, 2001; Rikhye et al., 2018b). In particular, comparative studies across all amniotes (reptiles, birds and mammals) have described a correlation between the proportion of interneurons and the size and connectivity of the excitatory thalamus (Arcelli et al., 1997; Butler, 2008).

For example, in the reptilian thalamus, which is mostly devoid of descending projections from the cortex, interneurons have only been identified in the retinorecipient regions (Rio et al., 1992; Pritz and Stritzel, 1994; Kenigfest et al., 1995, 1998; Butler, 2008). In birds however, where reciprocal connections between the thalamus and the cortex are more abundant, thalamic interneurons are distributed more widely (Granda and Crossland, 1989; Veenman and Reiner, 1994; Butler, 2008).

Similarly among mammals, interneurons are largely restricted to the visual thalamus in smaller-brained marsupials, bats and mice, where they represent only 6% of the total neuronal population (Butler, 2008; Evangelio, García-Amado and Clascá, 2018; Seabrook et al., 2013b). In primates, on the other hand, where higher order (HO) nuclei driven by cortical inputs are expanded relative to sensory relay (first order, FO) regions (Armstrong, 1979; Stephan, Frahm and Baron, 1981; Butler, 2008; Baldwin, Balaram and Kaas, 2017; Halley and Krubitzer, 2019), interneurons are present across the entire thalamus and their proportion increases to around 30% (Braak and Bachmann, 1985; Arcelli et al., 1997).

How could these differences arise as part of species-specific ontogenesis of thalamic interneurons? We have previously shown that in the mouse, interneurons in the FO visual thalamus, the dorsal lateral geniculate nucleus (dLGN), originate in the midbrain from an *En1*$^{+}$*Gata2*$^{+}$*Otx2*$^{+}$*Sox14*$^{+}$ lineage (Jager et al., 2016). On the other hand, earlier work in

humans has suggested the *DLX1/2*-expressing ganglionic eminences (GE) in the telencephalon as the source of interneurons for the HO thalamic nuclei - the mediodorsal nucleus and the pulvinar (Rakić and Sidman, 1969; Letinić and Kostović, 1997; Letinic and Rakic, 2001). At the same time, the latter studies were not able to detect any such migration from the GE in the mouse and macaque brain (Letinic and Rakic, 2001). Altogether these findings therefore suggest that innovation in developmental origin underlies the evolution of thalamic interneurons, concomitantly with an expanded cortical input to the thalamus. However, because each study considered different thalamic nuclei, and due to technical limitations, the possibility of evolutionary conservation of thalamic interneuron classes remains.

Here we hypothesised that in fact all mammals share a conserved developmental organization of thalamic interneurons, which becomes increasingly more elaborated in larger-brained species. This prediction is supported by findings from the cortex demonstrating that its interneuron classes, generated in the subpallium and defined through expression of regulatory programs (i.e. transcription factors), are common to the amniote lineages (Métin et al., 2007; Tasic et al., 2018; Tosches et al., 2018; Arendt et al., 2019). Moreover, a conserved subpallial origin was demonstrated for cortical interneurons in the cyclostome hagfish, and therefore appears to be an ancestral feature of the vertebrate brain (Sugahara et al., 2016, 2017).

Using mouse genetics together with *in situ* methods and spatial modeling, we investigated the distribution, transcription factor (TF) expression and ontogeny of thalamic GABAergic interneurons comprehensively across the mouse thalamocortical nuclei. These experiments identify a wider distribution of GABAergic interneurons than previously reported (Arcelli et al., 1997; Seabrook et al., 2013b; Evangelio et al., 2018), encompassing both FO sensory relay and HO thalamic nuclei. We then show that while the largest proportion of thalamic interneurons in the mouse is generated in the *En1*$^{+}$*Sox14*$^{+}$ embryonic midbrain, there is an additional class that derives from the *Dlx5*$^{+}$ inhibitory progenitor domains in the forebrain, potentially homologous to the one identified in humans. Intriguingly, we also find that interneurons are organized in a spatial pattern according to their ontogeny, such that midbrain-born interneurons are largely found in the sensory relay nuclei, while the forebrain-generated interneurons reside exclusively in the HO thalamus. Finally, we examined the evidence for midbrain-generated interneurons in the primate (marmoset) thalamus, and observed an abundant expression of corresponding marker genes.

Results

GABAergic cells are widely distributed across the mouse thalamus, with *Sox14* expression distinguishing between two spatially clustered classes

To investigate spatial and molecular diversity of interneurons comprehensively across all thalamic (thalamocortical, TC) regions in the mouse, we searched for markers by leveraging publicly available single-cell RNA sequencing data resources, and used mouse genetics together with *in situ* hybridization to anatomically map their expression.

In the mouse thalamus, GABAergic interneurons are most abundant in the dLGN (Arcelli et al., 1997; Evangelio et al., 2018). Both the Allen Brain Atlas (© 2015 Allen Institute for Brain Science. Allen Cell Types Database. Available from: celltypes.brain-map.org) and DropViz resources (Available from: dropviz.org; Saunders et al., 2018) identify a transcriptional cluster corresponding to mouse dLGN interneurons, and from this *Sox14* as one of transcription factor genes expressed selectively in the interneurons within the nucleus, confirming our previous findings (Jager et al., 2016). *Sox14* is expressed upon cell-cycle exit within inhibitory lineages in the diencephalon, midbrain, hindbrain and spinal cord, but not in the telencephalon (Delogu et al., 2012; Achim et al., 2013; Prekop et al., 2018; Guo and Li, 2019). We focused on a developmentally expressed transcriptional regulator with the assumption that cells of the same class/family would implement the same differentiation program (Deneris and Hobert, 2014; Tosches et al., 2018; Arendt et al., 2019).

We then mapped the spatial distribution of $Sox14^{+}$ cells within all TC regions using the $Sox14^{GFP/+}$ line (Crone et al., 2008), and compared it to that of the entire GABAergic population, labelled with *in situ* hybridization for *Gad1* (Fig. 1A-C). Experiments were done at postnatal day (P)14, by which time point mouse TC nuclei are considered to display adult-like circuit composition (Bickford et al., 2010; Golding et al., 2014; Seabrook et al., 2013a,b, 2017; Thompson et al., 2016).

In addition to the dLGN, $Sox14^{+}$ cells distributed across the LP, VP, PO and in very small numbers in the MG complex (Fig. 1A,C,D). In these nuclei all $Sox14^{+}$ cells had a GABAergic profile and co-expressed *Gad1* (100%, n=3 brains). In the dLGN, VP and MG (i.e. FO sensory relay nuclei) they also represented virtually all GABAergic cells (≥98%, pie charts in Fig. 1D).

Unexpectedly however, 22.1±4.0% of the total GABAergic population in TC regions did not express *Sox14* (Fig. 1B,C; 3Bii), and these cells appeared spatially largely non-overlapping with the $Sox14^{+}$ class (Fig. 1C,D). In particular, we observed the largest proportion of $Sox14^{-}$ $Gad1^{+}$ cells in the MD (29.6±4.5%), LD (19.4±3.1%) and LP (13.2±1.2%), and in smaller numbers in the CL, PO, VAL and VM (Fig. 1B,C,D).

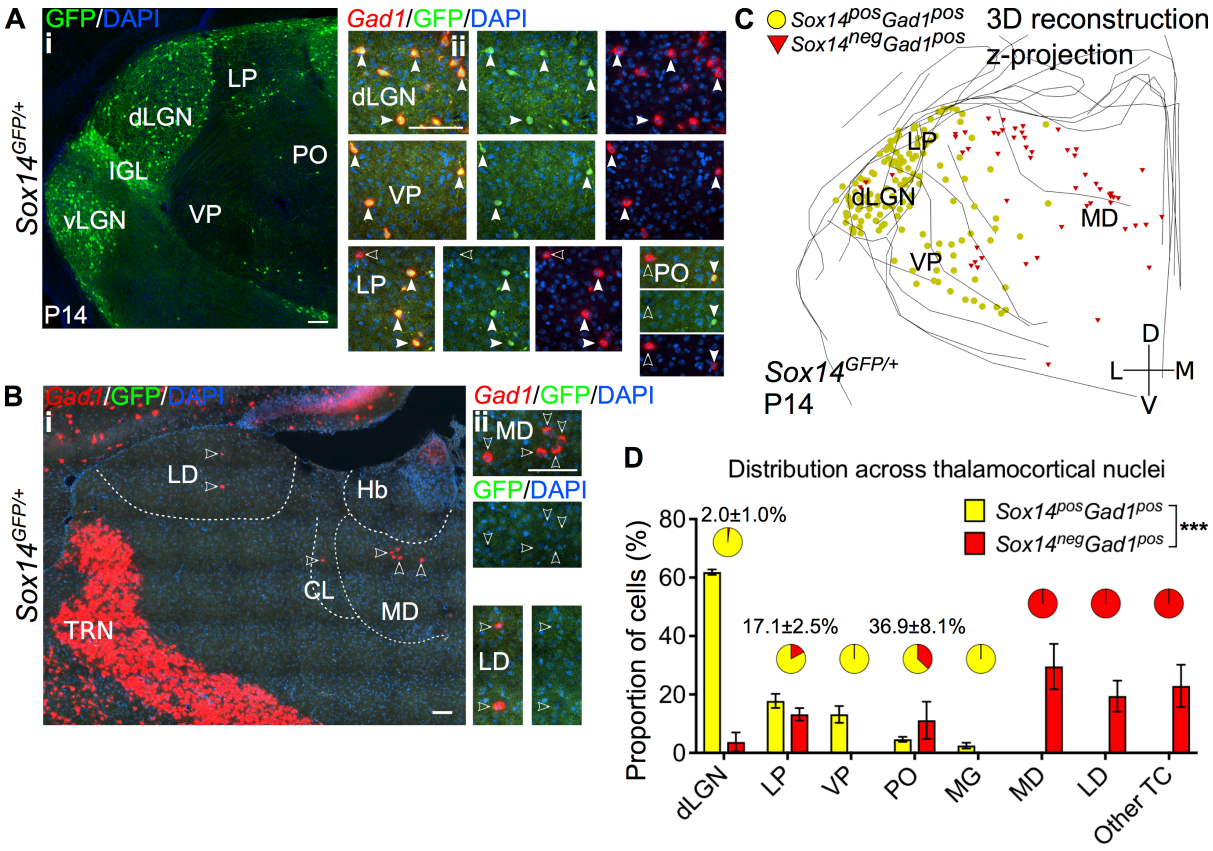

Figure 1. Diversity and distribution of GABAergic cells in the mouse thalamocortical nuclei. **A.** (i) Representative coronal section of P14 *Sox14*$^{GFP/+}$ thalamus with *Sox14*$^{+}$ cells in the dLGN, VP, LP and PO. (ii) *Sox14*$^{+}$ cells in TC regions co-express *Gad1*, but not all *Gad1*$^{+}$ cells co-express *Sox14* in the LP and PO. Filled arrows mark *Sox14*$^{+}$*Gad1*$^{+}$ and empty arrows *Sox14*$^{-}$*Gad1*$^{+}$ cells. Scale bars, 100 µm. **B.** (i) Representative rostral coronal section of P14 *Sox14*$^{GFP/+}$ thalamus with *Gad1*$^{+}$ cells in the MD, CL and LD, and containing no *Sox14*$^{+}$ cells. (ii) *Gad1*$^{+}$ cells in these nuclei do not co-express *Sox14*. Scale bars, 100 µm. **C.** 3D reconstruction of a representative P14 *Sox14*$^{GFP/+}$ thalamus from tracing every tenth 20µm-thick coronal section, displayed as a z-projection and showing distribution of *Sox14*$^{+}$*Gad1*$^{+}$ (yellow) and *Sox14*$^{-}$*Gad1*$^{+}$ cells (red). One dot represents one neuron. **D.** Distribution of *Sox14*$^{+}$*Gad1*$^{+}$ and *Sox14*$^{-}$*Gad1*$^{+}$ cells across TC nuclei in the *Sox14*$^{GFP/+}$ brains at P14, plotted as proportion of all the cells within each interneuron group (mean±SE; n= 3 brains). *Sox14*$^{+}$*Gad1*$^{+}$ and *Sox14*$^{-}$*Gad1*$^{+}$ populations have distinct distributions (p~0, Chi-squared test). Pie charts show the proportion (mean±SE) of the two interneuron classes within each nucleus.

To quantitatively demonstrate spatial clustering of these two putative thalamic interneuron classes (*Sox14*$^{+}$*Gad1*$^{+}$ and *Sox14*$^{-}$*Gad1*$^{+}$), we calculated the nearest neighbour distances (NND) from 3D reconstructions of their respective distributions in the *Sox14*$^{GFP/+}$ thalamus (Fig. 1C; 2A). Indeed, the cumulative distribution of NNDs was significantly shifted to smaller distances within each of the classes than between them ($p<1.4\times10^{-30}$, 2-sample Kolmogorov-Smirnov test, n=3 brains; Fig. 2A).

To characterise spatial organization of thalamic GABAergic interneurons in an unbiased way, we then applied machine learning (k-Means clustering) to these same 3D

reconstructions of the *Sox14*$^{GFP/+}$ thalami (Fig. 1C; 2B,C). The data best fit two spatial clusters, as assessed from the silhouette score (Fig. 2Bii,C; see also Materials and Methods). Consistent with the NND analysis, one cluster corresponded to the *Sox14*$^{+}$ cells (contains 94.9±1.4% of all *Sox14*$^{+}$ cells), and the other to the *Sox14*$^{-}$ interneurons (contains 81.0±0.3% of all *Sox14*$^{-}$ cells; Fig. 2B,D). The two thalamic molecular GABAergic groups therefore occupy their own respective spatial clusters, with the *Sox14*$^{-}$ cells located more rostrally and medially compared to the *Sox14*$^{+}$ interneurons.

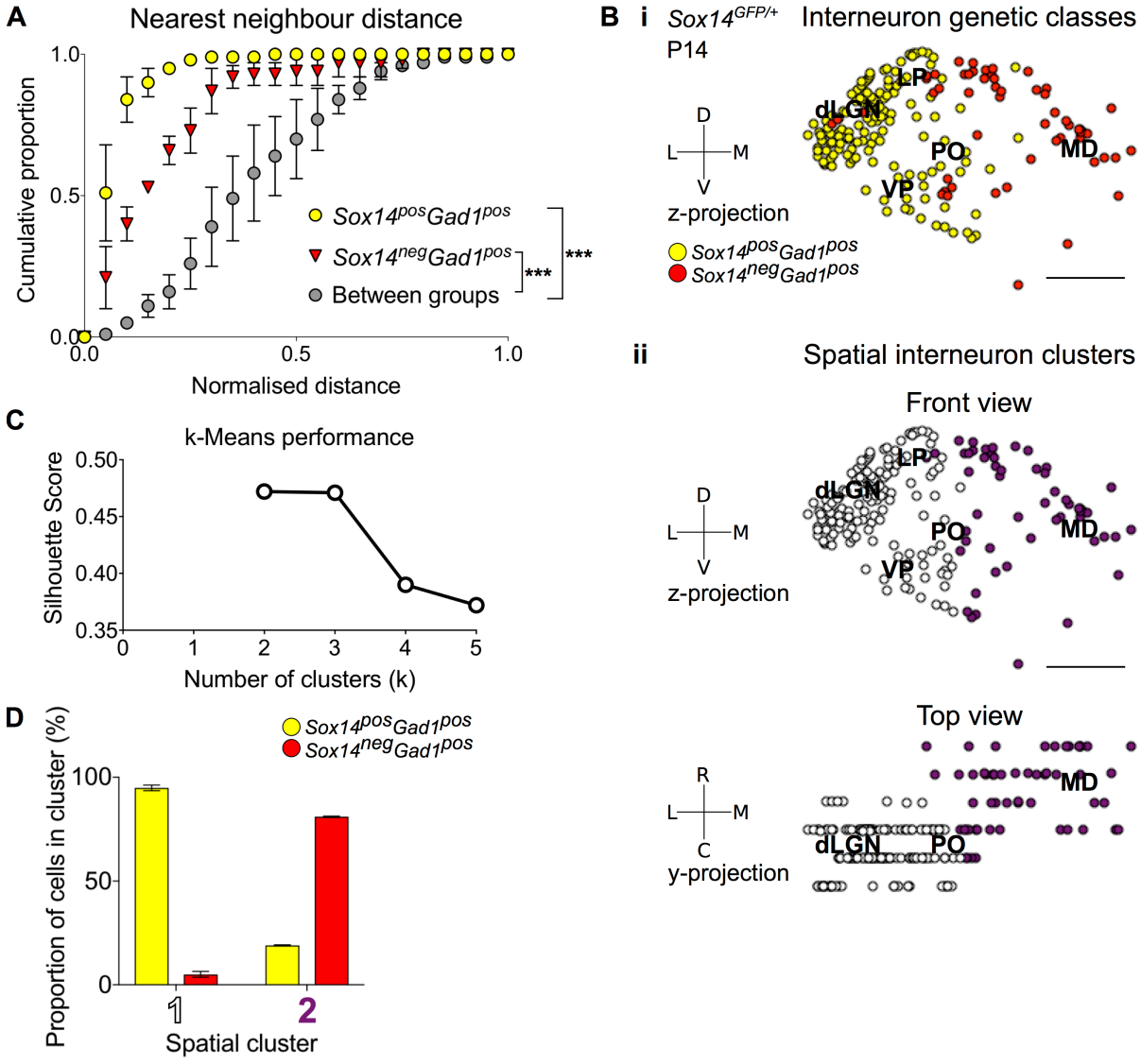

Figure 2. Spatial organization of thalamic GABAergic cells. **A.** Normalised nearest neighbour distance (NND) for *Sox14*$^{+}$*Gad1*$^{+}$ and *Sox14*$^{-}$*Gad1*$^{+}$ populations and between the two groups from P14 *Sox14*$^{GFP/+}$ data (Fig. 1), plotted as cumulative proportion of all cells within a given set. The NND distribution is significantly shifted to larger distances between groups than within each of the groups ($p<1.4\times10^{-30}$, 2-sample Kolmogorov-Smirnov test, n=3 brains). **B.** Representative z-projections of IN distribution amongst TC nuclei, from P14 *Sox14*$^{GFP/+}$ data (Fig. 1). One dot represents one neuron and they are colour-coded by (i) their genetic identity or (ii) spatial cluster. For the spatial clusters a y-projection is also

shown. Scale bars, 500µm. **C.** Performance of unsupervised k-Means algorithm in identifying thalamic interneuron spatial clusters from the P14 *Sox14*$^{GFP/+}$ data (n=3 brains, see also Fig. 1) as measured by the silhouette score, which varies with number of clusters (k). We choose k=2 as this point has the highest score. **D.** Proportion of *Sox14*$^{+}$ and *Sox14*$^{-}$ GABAergic cells in each spatial cluster, averaged over three brains (mean±SE).

To independently confirm our findings and control for potential effects of looking at a juvenile age (P14), we also mapped anatomical distribution of all *Gad1*$^{+}$ and *Chrna6*$^{+}$ cells across the adult mouse TC nuclei at P56, using the Allen Mouse Brain Atlas (© 2004 Allen Institute for Brain Science. Allen Mouse Brain Atlas. Available from: mouse.brain-map.org; Lein et al., 2006) *in situ* hybridization data (Supp. Fig. 1). *Chrna6* has been identified as another marker specific for interneurons, at least in the dLGN (Golding et al., 2014; DropViz; Allen Cell Types Database). The resulting 3D reconstructions, k-Means spatial clustering (Supp. Fig. 1A) and distribution plot (Supp. Fig. 1B) were consistent with our observations from the P14 *Sox14*$^{GFP/+}$ thalamus.

Mouse thalamus therefore exhibits wider interneuron distribution and diversity than has been previously reported, with at least two molecularly and spatially distinct classes. The largest interneuron class, which is distributed across FO and HO sensory nuclei including the dLGN, can be defined as *Sox14*$^{+}$. Conversely, the smaller *Sox14*$^{-}$ GABAergic population is found exclusively in HO regions that associate with more cognitive functions, such as the MD (Rikhye et al., 2018a; Halassa and Kastner, 2017).

All *Sox14*-expressing thalamic interneurons are born in the midbrain

We have previously shown that in the *Sox14*$^{GFP/GFP}$ (*Sox14* knockout, KO) there is a >90% reduction in the number of interneurons in the dLGN (Jager et al., 2016). Given the role of *Sox14* in specifying subcortical inhibitory classes (Delogu et al., 2012; Achim et al., 2013; Prekop et al., 2018; Guo and Li, 2019), this analysis was extended here to encompass all TC regions. We find a comparable reduction in the number of *Sox14*$^{+}$ interneurons overall across the dLGN, LP, VP, PO and MG in the *Sox14* KO (90.5±1.5%, $p=2.7\times10^{-4}$, two-sample two-tailed t-test, n=3 brains/genotype; Fig. 3A,B). Conversely, there was no significant change in the number of *Sox14*$^{-}$*Gad1*$^{+}$ cells (p=0.4, two-sample two-tailed t-test; Fig. 3A,B) and in their distribution across TC regions (Fig. 3A,C; p>0.05, Chi-squared test, n=3 brains/genotype). These results therefore indicate that the two TC interneuron populations may already be segregated during development and represent two non-overlapping GABAergic lineages.

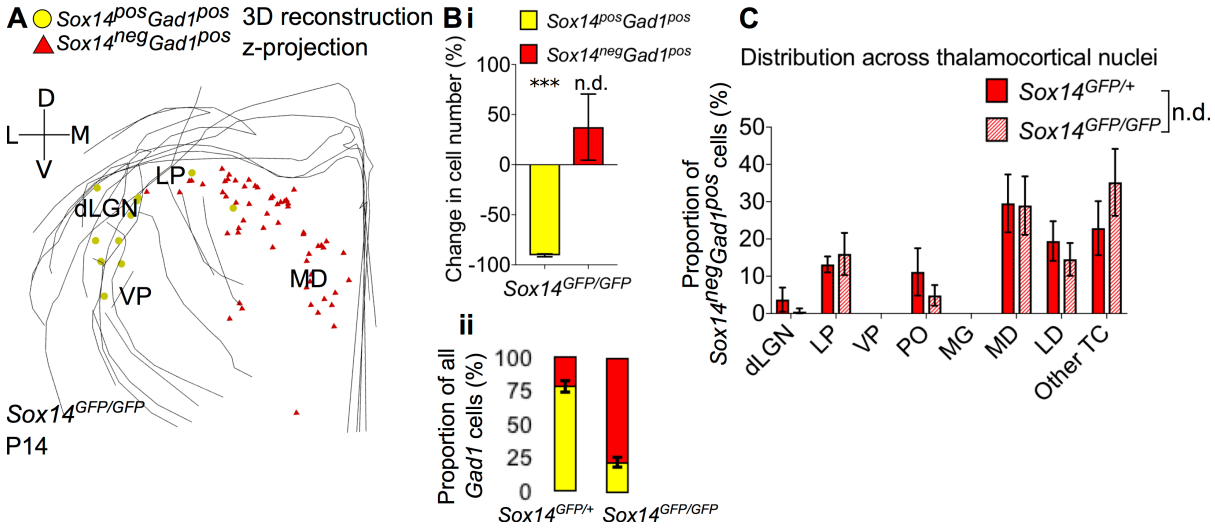

Figure 3. A. 3D reconstruction of a representative P14 *Sox14*$^{GFP/GFP}$ thalamus from tracing every tenth 20µm-thick coronal section, displayed as a z-projection and showing distribution of *Sox14*$^{+}$*Gad1*$^{+}$ (yellow) and *Sox14*$^{-}$*Gad1*$^{+}$ cells (red). **B.** (i) Relative change in the number of *Sox14*$^{+}$*Gad1*$^{+}$ and *Sox14*$^{-}$*Gad1*$^{+}$ cells across TC regions in P14 *Sox14*$^{GFP/GFP}$ relative to P14 *Sox14*$^{GFP/+}$ data (mean±SE, n=3 brains/genotype). There is a significant reduction in the *Sox14*$^{+}$*Gad1*$^{+}$ population ($p=2.7\times10^{-4}$, two-sample two-tailed t-test), but no statistically significant difference in the size of the *Sox14*$^{-}$*Gad1*$^{+}$ group (p=0.4, two-sample two-tailed t-test). (ii) Proportion of *Sox14*$^{+}$*Gad1*$^{+}$ cells within the total GABAergic population is decreased in the *Sox14*$^{GFP/GFP}$ (mean±SE, n=3 brains/genotype). **C.** Distribution of *Sox14*$^{-}$*Gad1*$^{+}$ cells across TC nuclei in the *Sox14*$^{GFP/+}$ and *Sox14*$^{GFP/GFP}$ brains at P14 (mean±SE; n= 3 brains/genotype). *Sox14*$^{-}$*Gad1*$^{+}$ distribution is unaltered in the *Sox14* KO (p>0.05, Chi-squared test).

dLGN interneurons in the mouse derive from the midbrain (Jager et al., 2016). To explore how the molecular and spatial organization of thalamic interneurons is generated during development more conclusively, we fate-mapped midbrain lineages and checked for their presence, distribution and inhibitory profile across the thalamus. We crossed *En1-Cre* (Kimmel et al., 2000) with a *R26lsl-GFP* (Sousa et al., 2009) reporter line (Fig. 4A), as the *En1* TF gene is expressed in the midbrain and rostral hindbrain progenitors, but not in the forebrain (Sgaier et al., 2007). The analysis was done at P21-30 and, confirming our previous findings, there were GFP^{+} cells (*En1*$^{+}$ lineage) distributed across the dLGN and co-expressing GABA (Fig. 4B). However, like the *Sox14*$^{+}$*Gad1*$^{+}$ neurons, *En1*$^{+}$ cells were observed beyond the dLGN - in the LP, VP, PO and MG, where they were also positive for GABA (Fig. 4B,C). Plotting their distribution confirmed that it is equivalent to *Sox14*$^{+}$ interneurons (p>0.05, Chi-squared test; Fig. 4C,D). Occasional GFP^{+} cells with glia-like morphology were also observed in the thalamus. These cells were GABA^{-} and were not included in any of the analyses.

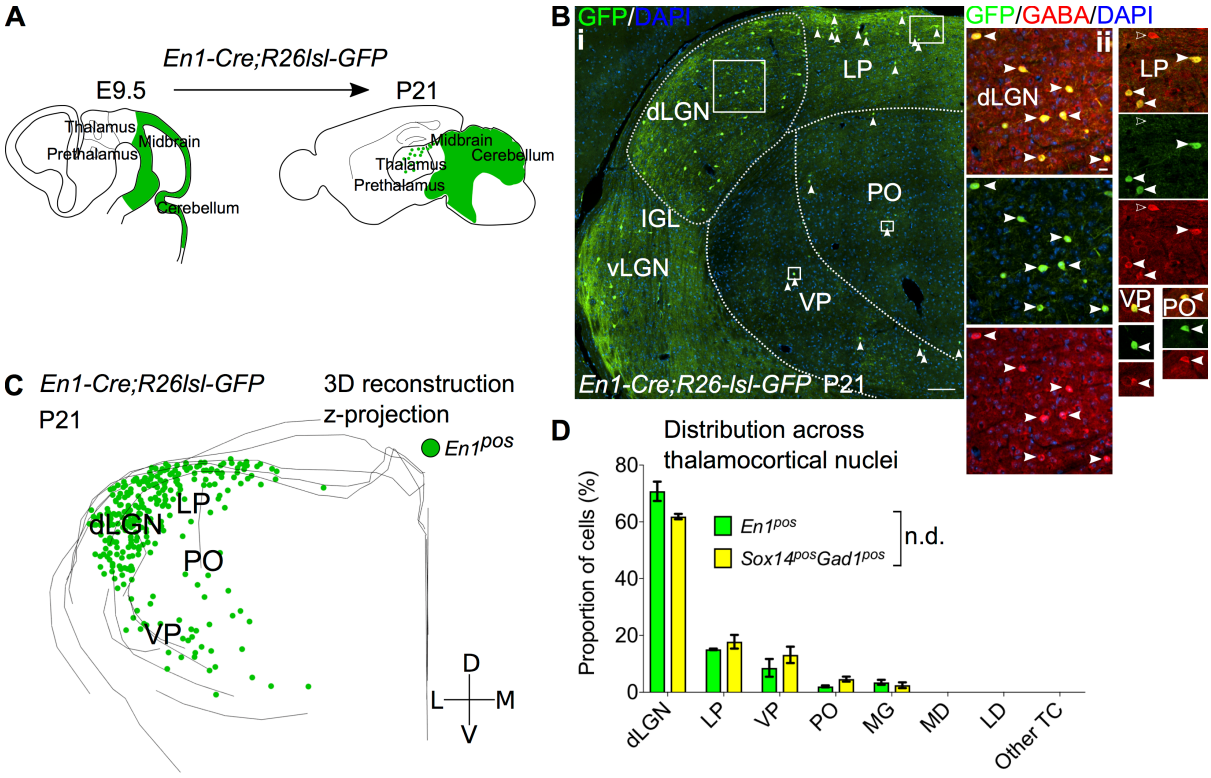

Figure 4. *Sox14*$^{+}$ interneurons in TC regions derive from the midbrain. **A.** Schematic of the fate mapping experiment: crossing *En1-Cre* with *R26lsl-GFP* reporter line permanently labels all midbrain born cells with GFP expression. **B.** (i) Representative coronal section of P21 *En1-Cre;R26lsl-GFP* thalamus with *En1*$^{+}$ cells observed in the dLGN, LP, VP and PO (considering TC regions only). For clarity some of the *En1*$^{+}$ cells are indicated with white arrows. Scale bar, 100µm. (ii) *En1*$^{+}$ cells in these regions co-express GABA (filled white arrows). Empty arrows mark GABA single-positive cells. Scale bar, 10µm. **C.** 3D reconstruction of a representative P21 *En1-Cre;R26lsl-GFP* thalamus from tracing every sixth 60µm-thick coronal section, displayed as a z-projection and showing distribution of *En1*$^{+}$ cells. **D.** Distribution of *Sox14*$^{+}$*Gad1*$^{+}$ and *En1*$^{+}$ cells across TC nuclei in *Sox14*$^{GFP/+}$ and *En1-Cre;R26lsl-GFP* brains, respectively, plotted as proportion of all the cells within each group (mean±SE; n= 3 brains/genotype). The two populations are not differently distributed (p>0.05, Chi-squared test).

We therefore conclude that the *Sox14*$^{+}$ thalamic interneurons derive from the midbrain, and simultaneously that the *Sox14*$^{-}$ GABAergic cells do not; the two classes thus represent distinct inhibitory lineages in TC regions, further supporting their definition as two distinct thalamic interneuron classes.

Midbrain-derived interneurons migrate into the sensory thalamus in the first postnatal week in two streams

En1-Cre;R26lsl-GFP line was then used to investigate the timeline and spatial trajectories of the *Sox14*$^{+}$ interneuron precursors migrating from the midbrain into the first and higher order sensory TC regions (Fig. 5A). Previously, dLGN interneurons were found to populate this nucleus in the first postnatal week (Golding et al., 2014; Jager et al., 2016). We therefore

looked at the numbers and migratory morphology of GFP$^+$ (i.e. *En1*$^+$) cells in the thalamus at E16.5, E17.5, P0.5, P1.5 and P2.5. We focused on the dLGN, LP and VP, but left out the PO and MG, due to low overall numbers of interneurons in these two regions in the juvenile/adult mouse thalamus (Fig. 1, Supp. Fig. 1).

At E16.5 no GFP$^+$ cells were present in the thalamus. From E17.5 to P2.5 their numbers progressively increased in all of the regions analysed (Fig. 5A,B). The number of GFP$^+$ cells in the dLGN at P2.5 matched previous independent reports (Golding et al., 2014), validating our counting method. Midbrain-derived interneurons therefore populate the different TC regions following a similar timeline. Interestingly, they appear in two ventrally located nuclei (i.e. dLGN and VP) simultaneously (Fig. 5A,B), implying they use distinct routes to reach them.

To infer their direction of migration, we determined the leading process orientation of migrating GFP$^+$ cells along all three dimensions (ventro-dorsal, latero-medial, caudo-rostral; Fig. 5C; Jager et al., 2016; Paredes et al., 2016). This was plotted at a population level as frequency distribution using heat maps, for each nucleus individually, for E17.5 and P0.5 (Fig. 5D; Supp. Fig. 2B), as the relative increase in GFP$^+$ cell numbers was the greatest between these two timepoints (Fig. 5B). Moreover, there was a progressive decrease across developmental stages in the proportion of GFP$^+$ cells for which migratory morphology could be identified (Supp. Fig. 2A).

Heat maps indicate that at a population level (integrated across dimensions), GFP$^+$ cells migrate into the dLGN, LP and VP in a caudo-rostral and dorso-ventral direction (Fig. 5D), consistent with the position of the thalamus in the brain relative to their midbrain origin. However, GFP$^+$ precursors in the dLGN and LP have a dominant medio-lateral orientation, while those in the VP an opposite, latero-medial orientation, as can also be seen from polar histograms (Supp. Fig. 2C). This suggests that midbrain-derived interneuron precursors enter TC regions simultaneously in two distinct streams, one migrating rostro-ventro-laterally to the dLGN and LP, and the other rostro-ventro-medially to the VP, indicating a split between visual (dLGN, LP) and somatosensory (VP) TC nuclei.

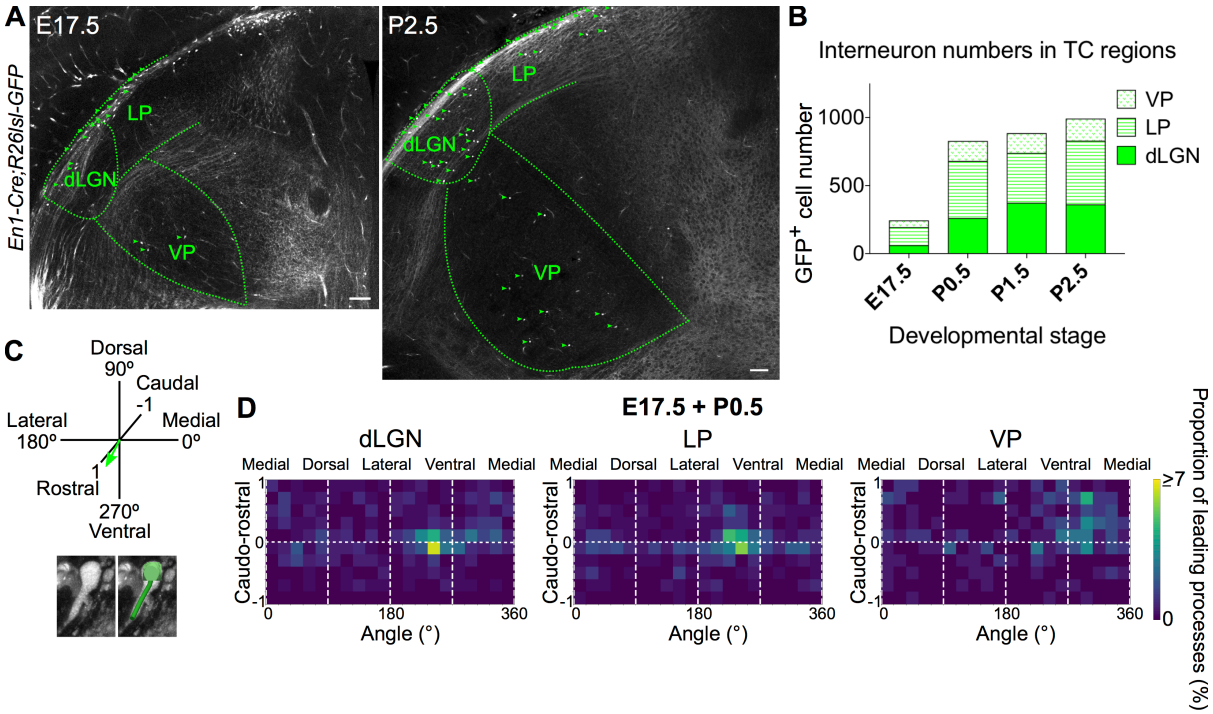

Figure 5. Midbrain-derived interneuron precursors progressively populate the thalamus from E17.5 onwards. **A.** Representative coronal sections of *En1-Cre;R26lsl-GFP* thalamus at E17.5 and P2.5. Green arrows mark some of the GFP$^+$ cells. Scale bars, 100µm. **B.** Number of GFP$^+$ cells counted in the dLGN, LP and VP from E17.5 to P2.5 (mean, n=3 brains). **C.** Leading process orientation of GFP$^+$ cells was determined along the caudo-rostral, ventro-dorsal and latero-medial dimensions. **D.** Frequency distribution of leading process orientation for GFP$^+$ cells in the dLGN, LP and VP at E17.5 and P0.5 combined, represented in heat maps (n=3 brains/developmental stage).

Sox14-negative thalamic interneurons populating higher order nuclei are born in the forebrain

Having excluded the midbrain, we aimed to identify the origin of the *Sox14*$^-$ interneuron class in the mouse HO TC regions. To molecularly define it, we made use of DropViz data (Available from: dropviz.org; Saunders et al., 2018) and observed that within inhibitory clusters from the thalamus and surrounding regions, *Sox14* and *Pvalb* show largely non-overlapping expression, where *Pvalb* is a marker for at least 5 out of 11 inhibitory clusters (Pvalb p-value< $9.05e^{-30}$). It is known that *Pvalb* is expressed by the nearby prethalamic structures like the thalamic reticular nucleus (TRN; Clemente-Perez et al., 2017), and by telencephalic interneuron types derived from the ganglionic eminences (Marin and Rubenstein, 2001; Tremblay, Lee and Rudy, 2016; Tasic et al., 2016).

We therefore crossed *Pv-Cre* (Hippenmeyer et al., 2005) with a *R26lsl-nuclearGFP* (Mo et al., 2015) reporter line to label *Pvalb*$^+$ cells, and assessed their distribution and GABAergic profile in TC nuclei at P14 (Supp. Fig. 3A). *Pvalb*$^+$ cells were present in regions populated by the *Sox14*$^-$ interneurons, including the MD, LD, LP and PO, and absent from the nuclei populated exclusively by *Sox14*$^+$ interneurons, such as the dLGN and VP (Supp. Fig. 3Ai).

At later ages (P56) *Pvalb* is widely expressed in the thalamus, and is observed in high-density gradients in several nuclei, including the VP (© 2004 Allen Institute for Brain Science. Allen Mouse Brain Atlas. Available from: mouse.brain-map.org; Lein et al., 2006). Importantly however, at P14 93.9% of *Pvalb*$^+$ cells in TC regions co-expressed GABA (n=2 brains, Supp. Fig. 3Aii,B). Therefore, we define the *Sox14*$^-$ GABAergic cells as *Pvalb*$^+$, and restricted our analyses to P14.

Previous reports suggested the *DLX1/2/5*$^+$ ganglionic eminences (GE) as a source of thalamic interneurons in humans (Rakić and Sidman, 1969; Letinić and Kostović, 1997; Letinic and Rakic, 2001). We investigated this possibility directly and fate-mapped the progeny from forebrain inhibitory progenitor domains in the mouse thalamus, by crossing *Dlx5-Cre* (Monory et al., 2006) to *R26lsl-GFP* line (Fig. 6A).

At P14 all TC Pvalb$^+$ cells are a *Dlx5* lineage (GFP$^+$; 100%, n=3 brains; Fig. 6B,Ci) and majority of them co-expressed GABA (93.6±3.7%; Fig. 6Cii), in line with observations from the *Pv-Cre;R26lsl-nGFP* line (Supp. Fig. 3Aii,B).

We also observed Pvalb$^-$*Dlx5*$^+$ cells in the thalamus, the majority of which had a glia-like morphology and did not express GABA (Supp. Fig. 3C). Occasional Pvalb$^-$GABA$^-$*Dlx5*$^+$ cells with neuronal-like morphology were also seen (Supp. Fig. 3C,D), suggesting leaky Cre activity in some cases. That all Pvalb$^+$GABA$^+$ cells in TC nuclei are labelled with GFP argues against this being an artefact of leaky reporting. Pvalb$^-$GABA$^-$*Dlx5*$^+$ cells were not considered in any of the analyses.

Finally, we mapped the distribution of Pvalb$^+$*Dlx5*$^+$ cells across TC regions (Fig. 6D,E) and observed that it matches the *Sox14*$^-$*Gad1*$^+$ cells (Fig. 6E; $p>0.05$, Chi-squared test). Altogether, we therefore conclude that the *Sox14*$^-$*Pvalb*$^+$ thalamic interneurons originate from *Dlx5*$^+$ inhibitory progenitors domains located in the forebrain, emphasizing their distinct lineage compared to the larger, midbrain-born *Sox14*$^+$ thalamic interneuron class.

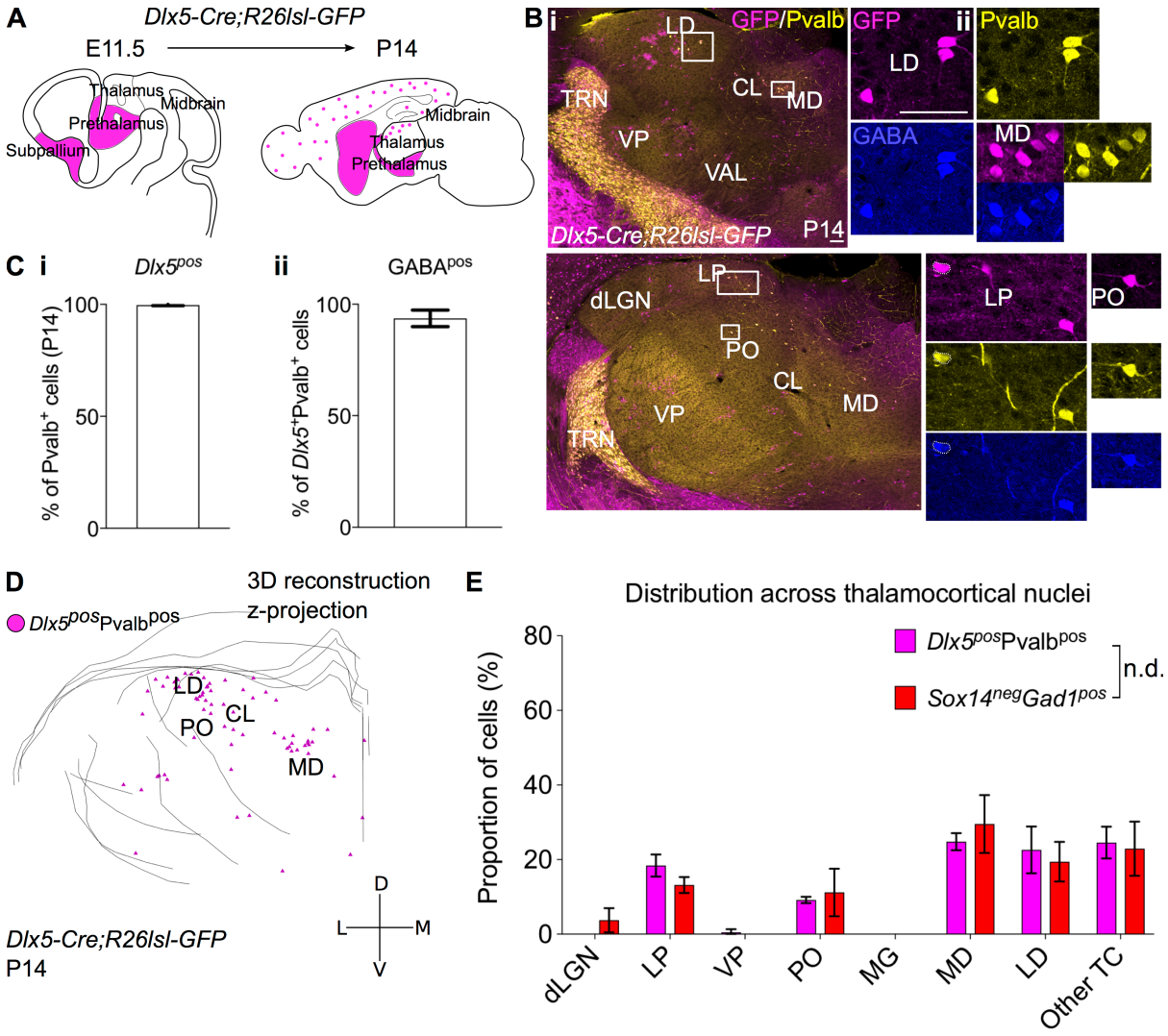

Figure 6. *Sox14*$^{-}$*Pvalb*$^{+}$ interneurons in TC regions derive from the rostral forebrain. **A.** Schematic of the fate mapping experiment: crossing *Dlx5-Cre* with *R26lsl-GFP* reporter line permanently labels all ventral telencephalic and prethalamic-born cells with GFP expression. **B.** (i) Representative coronal sections of P14 *Dlx5-Cre;R26lsl-GFP* thalamus with *Dlx5*$^{+}$Pvalb^{+} cells present in the MD, LD, CL, VAL, VM, LP and PO (considering TC regions only). Scale bar, 100µm. (ii) *Dlx5*$^{+}$Pvalb^{+} cells in TC regions co-express GABA. Scale bar, 100µm. **C.** (i) Proportion of Pvalb^{+} cells in TC regions that are *Dlx5*$^{+}$ at P14 (mean±SE, n=3 brains). (ii) Proportion of *Dlx5*$^{+}$Pvalb^{+} cells in TC regions co-expressing GABA at P14 (mean±SE, n=3 brains). **D.** 3D reconstruction of a representative P14 *Dlx5-Cre;R26lsl-GFP* thalamus from tracing every sixth 60µm-thick coronal section, displayed as a z-projection and showing distribution of *Dlx5*$^{+}$Pvalb^{+} cells. **E.** Distribution of *Dlx5*$^{+}$Pvalb^{+} and *Sox14*$^{-}$*Gad1*$^{+}$ cells across TC nuclei in P14 *Dlx5-Cre;R26lsl-GFP* and *Sox14*$^{GFP/+}$ brains, respectively, plotted as proportion of all the cells within each group (mean±SE, n= 3 brains/genotype). The two populations are not differently distributed (p>0.05, Chi-squared test).

The presence of a *Dlx5*$^{+}$ inhibitory lineage in the mouse thalamus is therefore consistent with the proposed ontogeny for human thalamic interneurons (Rakić and Sidman, 1969; Letinić and Kostović, 1997; Letinic and Rakic, 2001). Correspondingly, we investigated if the midbrain-derived interneurons identified in mouse could also be found in the primate

thalamus. We used the Marmoset Gene Atlas to examine the expression of *SOX14* and *OTX2*, known markers for the mouse dLGN interneurons (Golding et al., 2014; Jager et al., 2016; DropViz), in the early postnatal marmoset thalamus. These were then compared to the *GAD1* signal (all ISH data available from: https://gene-atlas.brainminds.riken.jp; Shimogori et al., 2018).

This shows that both *SOX14*$^+$ and *OTX2*$^+$ cells are present across all marmoset thalamocortical nuclei (Supp. Fig. 4A), with a similar distribution and density to the *GAD1*$^+$ neurons (Supp. Fig. 4B), seemingly accounting for the majority of GABAergic cells in the marmoset dorsal thalamus. On the other hand, forebrain-derived prethalamic inhibitory structures like the reticular nucleus are negative for the two markers (Supp. Fig. 4A).

Discussion

Our study reveals a previously unappreciated complexity in the GABAergic interneuron population distributed across the mouse thalamocortical nuclei.

In particular, we describe two broad thalamic interneuron classes, defined by (1) expression of transcription factors that are part of distinct regulatory programmes of GABAergic specification (*Sox14*$^+$ vs *Dlx5*$^+$; Eisenstat et al., 1999; Marin and Rubenstein, 2001; Stühmer et al., 2002; Achim et al., 2013, 2014; Mayer et al., 2018; Mi et al., 2018; Arendt et al., 2019), and (2) their origin in the midbrain and forebrain, respectively.

As expected, interneuron numbers and density were largest in the dLGN. We then show that one of the markers for the dLGN interneurons, the *Sox14* transcriptional regulator, labels GABAergic cells found scattered across all first and higher order sensory nuclei (dLGN, LP, VP, PO and MG; Guillery and Sherman, 2002; Wang, Eisenback and Bickford, 2002; Pouchelon et al., 2014; Roth et al., 2015; Frangeul et al., 2016). Using fate-mapping, we demonstrate that in all of these regions *Sox14*$^+$ interneurons derive from *En1*$^+$ midbrain and migrate into the thalamus late embryonically. This is in contrast to the broadly spatially separated *Sox14*$^-$ interneurons, representing around 20% of the total thalamic interneuron population. The *Sox14*$^-$ class is found exclusively in HO thalamocortical nuclei (e.g. the MD, LD, LP and PO; Sherman, 2016; Halassa and Kastner, 2017), can be defined as Pvalb$^+$ and originates from *Dlx5*$^+$ inhibitory progenitor domains in the forebrain.

These results reconcile discrepant findings on the origin of thalamic interneurons. For example, ganglionic eminence-derived *DLX1/2*$^+$ interneurons were shown to migrate into human MD and pulvinar (Rakić and Sidman, 1969; Letinić and Kostović, 1997; Letinic and Rakic, 2001), as opposed to the midbrain origin that we previously identified for the mouse dLGN interneurons (Jager et al., 2016). Our study suggests these different observations

could be the result of spatial segregation of ontogenetic interneuron classes, which may in fact be conserved across mammals.

Supporting this conclusion, gene expression evidence from the marmoset indicates that midbrain-generated interneurons are also present in the primate thalamus. Similarly, Jones (2002) and Hayes et al. (2003) previously described late appearance of interneurons in the ferret and macaque thalamus, progressively from caudal towards rostral nuclei. It can also be seen from the BrainSpan Atlas of the Developing Human Brain (© 2010 Allen Institute for Brain Science. BrainSpan Atlas of the Developing Human Brain. Available from: www.brainspan.org; Miller et al., 2014) that both *GAD1* and *SOX14* expression increase in the dorsal thalamus in the mid-prenatal period (from postconception week 16), which would be consistent with a migration of midbrain-born interneurons into these regions.

Interestingly, grafting experiments using chick and quail embryos demonstrated a potential for midbrain cells to populate retino-recipient nuclei in the chick diencephalon (Martinez and Alvarado-Mallart, 1989). The grafted midbrain cells were observed migrating tangentially at the surface of the diencephalon and seemingly through the host optic tract before invading the regions targeted by the retinal projections (Martinez and Alvarado-Mallart, 1989). The neurotransmitter identity of these migrating cells is unknown, but their midbrain origin and distribution across the thalamus resemble the mouse *Sox14*$^{+}$ interneurons, suggesting that in birds too, interneurons in the visual thalamus are a midbrain lineage. Relatedly, lineage tracing in chick, using a retroviral library, indicated that clonally related siblings can populate both the diencephalon and mesencephalon (Golden and Cepko, 1996).

In the future, it would be important to conclusively address how thalamic interneurons evolved by comparing their diversity and origin comprehensively across amniotes, as was recently done for cortical interneurons (Tosches et al., 2018; Tasic et al., 2016, 2018).

Finally, it is intriguing that in the mouse spatial organization of interneuron classes appears to correlate with anatomical and functional organization in the thalamus, which sees a split between sensory relay and higher order processing (Guillery and Sherman, 2002; Sherman, 2016; Halassa and Kastner, 2017). Here we provide genetic definitions and origin for the two broad thalamic interneuron classes, which can be used to investigate the functional significance of local inhibition in TC computations underlying both sensory perception and cognition.

Materials and Methods

Animals

Species	Designation	Source or reference	Identifiers	Additional information
Mus musculus	Sox14^{tm1Tmj} (Sox14eGFP)	Crone et al., 2008	MGI ID: 3836003	Maintained in the C57BL/6J (Charles River Laboratories) background
Mus musculus	En1-Cre	Kimmel et al., 2000; The Jackson Laboratory	Stock No: 007916 MGI ID: 2446434	C57BL/6J background
Mus musculus	Dlx5/6-Cre	Monory et al., 2006; The Jackson Laboratory	Stock No: 008199; MGI ID:3758328	C57BL/6J background
Mus musculus	B6 PV^{cre}	Hippenmeyer et al., 2005; The Jackson Laboratory	Stock No: 017320; MGI ID:3590684	C57BL/6J background
Mus musculus	RCE:loxP	Sousa et al., 2009; The Jackson Laboratory	MMRRC Stock No: 32037-JAX MGI:4412373	C57BL/6J background
Mus musculus	Gt(ROSA)26Sortm5(CAG-Sun1/sfGFP)Nat	Mo et al., 2015; The Jackson Laboratory	Stock No: 021039; MGI ID: 5443817	C57BL/6J background

Table 1: Mouse strains used in the study.

The mice were housed in the animal facilities at King's College London under standard conditions on a 12h:12h dark/light cycle, with unrestricted access to water and food. Housing and experimental procedures were approved by the King's College London Ethical Committee and conformed to the regulations of the UK Home Office personal and project licences under the UK Animals (Scientific Procedures) 1986 Act. Both female and male mice were used in a randomised way across experiments. The morning when the vaginal plug was observed was designated as embryonic day (E) 0.5 and the day of birth as postnatal day (P) 0.5.

Immunohistochemistry and *in situ* hybridization

Mice were transcardially perfused with 4% PFA and the brains dissected and postfixed in PFA at 4°C overnight, then washed in PBS for at least 24 hours at 4°C. For *in situ* hybridization (ISH), brains were stored in PFA for 5 days, to minimise RNA degradation, and all the subsequent solutions were treated with diethyl pyrocarbonate (DEPC; AppliChem). The brains were cryoprotected in a sucrose gradient (10–20– 30%), frozen on dry ice and cryosectioned as 20µm coronal sections collected on Superfrost Ultra Plus slides (Thermo

Scientific) for ISH, or as 60µm free-floating coronal sections for IHC.

Immunohistochemistry

Antibody	Dilution	Incubation time	Source
Rabbit anti-GABA	1:2000	2X ON, 4ºC	Sigma, A2052
Chicken anti-Gfp	1:5000	2X ON, 4ºC	Abcam, Ab13970
Mouse anti-Parvalbumin	1:2000	1X ON, 4ºC	Sigma-Aldrich, P3088
Goat anti-chicken Alexa-488	1:500	2h, RT	Invitrogen, A11039
Goat anti-rabbit Alexa-568	1:500	2h, RT	Invitrogen, A11036
Goat anti-rabbit Alexa-647	1:500	2h, RT	Invitrogen, A21245
Goat anti-mouse Alexa-568	1:500	2h, RT	Invitrogen, A11004
Goat anti-mouse Alexa-635	1:500	2h, RT	Invitrogen, A31575

Table 2: Antibodies

Brain sections were washed in PBS three times and blocked in 2-7% normal goat serum (NGS) solution (in 1X PBS, 0.1-0.3% Triton-X100) for 2 hours at room temperature (RT). Primary antibodies (Table 2) were diluted in blocking solution and incubated with the sections (as stated in the table). This was followed by three 30min PBS washes, and incubation in secondary antibodies (Table 2) diluted 1:500 in blocking solution, for 2 hours at RT. After two 30min PBS washes, the sections were incubated in DAPI for 30 min (1:40000 dilution in PBS; Life Technologies), and mounted using ProLong Gold mounting media (Invitrogen).

In situ hybridization

Gad1 antisense RNA probe was transcribed *in vitro* from full-length cDNA template (IMAGE ID: 5358787). The probe was diluted to a final concentration of 800ng/ml in hybridization buffer (50% formamide, 10% dextran sulphate, 1mg/ml rRNA, 1X Denhardt's solution, 0.2M NaCl, 10mM Tris HCl, 5mM $NaH_2PO_4.2H_2O$, 1mM Tris base, 50mM EDTA) and applied onto the slides, which were incubated in a humidified chamber at 65°C overnight. The slides were then washed three times for 30min in wash buffer (50% formamide, 1X SSC, 0.1% Tween) at 65°C, two times for 30min in MABT buffer (100mM maleic acid, 150mM NaCl, 0.1% Tween-20) at RT, and blocked for 2h at RT (2% Boehringer Blocking Reagent (Roche), 20% inactivated sheep serum in MABT). Sheep a-DIG alkaline phosphatase conjugated antibody (Roche, 11093274910) was diluted 1:2000 in the blocking solution and incubated with the slides overnight at 4°C. This was followed by five 20min washes in MABT and two 20min washes in the AP buffer (0.1M Tris-HCl pH8.2, 0.1%-Tween-20). Fast red TR/Naphthol AS-MX tablets (Sigma) were dissolved in the AP buffer and applied onto the slides for colour reaction for 3–6 hours at RT in the dark. The slides were then washed three times for 20min in PBS before proceeding with IHC for GFP as described above. *Sox14*$^{GFP/+}$ and *Sox14*$^{GFP/GFP}$ sections were always processed in parallel.

Quantifying distribution of neuronal populations across thalamic nuclei

Transgenic line	Age	Cells annotated/counted	Number of brains	Sampling	Section thickness (µm)
Sox14$^{GFP/+}$	P14	GFP$^+$ and *Gad1*$^+$	3	Every 10th coronal section	20
Sox14$^{GFP/GFP}$	P14	GFP$^+$ and *Gad1*$^+$	3	Every 10th coronal section	20
En1-Cre;R26lsl-GFP	P21-30	GFP$^+$	3	Every 6th coronal section	60
Dlx5/6-Cre;R26lsl-GFP	P14	GFP$^+$, Pvalb$^+$ and GABA$^+$	3	Every 6th coronal section	60
Pv-Cre;R26lsl-nGFP	P14	GFP$^+$, Pvalb$^+$ and GABA$^+$	2	Every 6th coronal section	60

Table 3. Genetic identity of cells counted across TC regions and technical details of corresponding experiments.

Confocal z-stacks covering the extent of the thalamus across all axes (caudo-rostral, ventro-dorsal, latero-medial) were acquired using either Nikon A1R inverted confocal, inverted spinning disk Nikon Ti microscope or Olympus VS120 slide scanner, with 10X (NA 0.30 Plan Fluor DLL) and 20X (NA 0.75 Plan Apo VC or UPLSAPO NA 0.75) objectives. The stacks were then viewed with the Neurolucida software. TC nuclei were identified from the DAPI counterstain, using cytoarchitectonically recognizable structures, such as the dLGN, the habenular complex, the TRN, the anterior pretectum and the fasciculus retroflexus (fr), as landmarks for orientation and reference. The cells of interest (Table 3) were assigned to TC regions by comparing the sections to the Allen Brain Reference Atlas and annotated and counted manually. For each brain, only one hemisphere was analysed (chosen in a randomized way). For experiments using *Gad1*$^+$ and *Chrna6*$^+$ *in situ* hybridization data from the Allen Mouse Brain Atlas resource (© 2004 Allen Institute for Brain Science. Allen Mouse Brain Atlas. Available from: mouse.brain-map.org; Lein et al., 2006), all images of P56 C57BL/6J coronal brain sections containing the thalamus were downloaded for each gene (every 8th 25µm-thick section, sampling every 200µm across the thalamus), and analysed in the same way as described above.

3D reconstructions of cell distributions

3D reconstructions of cell (Table 3) distributions across thalamic regions were generated for each brain separately using the Neurolucida software (MBF Bioscience), from the acquired confocal z-stacks or Allen Mouse Brain Atlas *in situ* hybridization data as described above. For each image the outline of the thalamus and the surrounding structures was manually traced using the 'contour' function and the cells were annotated with the 'marker' function, placed at the centre of the soma. Traced images were then aligned in sequential rostro-caudal order, manually for each brain, using tissue landmarks (midline and clearly recognisable structures, e.g. dLGN, TRN, habenula, hippocampus) for reference, and their

spacing in the rostro-caudal dimension was preserved according to the sampling used for each brain.

Nearest Neighbour Distance calculations

Nearest neighbour distance (NND) was determined for the *Sox14*$^{+}$*Gad1*$^{+}$ and *Sox14*$^{-}$*Gad1*$^{+}$ cells from the 3D reconstructions of their distributions. The cells' coordinates in 3D were generated by Neurolucida and analysed using a custom Python script and the Pandas library (McKinney, 2010) to calculate NNDs separately for each group and between the two groups, for each *Sox14*$^{GFP/+}$ brain individually. The data was then normalised to the largest NND within each data set (each individual group and between groups sets for each brain), averaged across the brains (mean±SE) and plotted as cumulative distribution. Normalization allows us to plot their cumulative distribution as a fraction of the maximum distance, though even before normalization the curves were broadly similar. Statistically significant differences between the distributions were verified using the 2-sample Kolmogorov-Smirnov test, implemented in the SciPy library (Jones et al.).

Migrational morphology analyses

E16.5, E17.5, P0.5, P1.5 (n=3 brains/developmental stage) and P2.5 (n=1) *En1-Cre;R26lsl-GFP* brains were quickly dissected on ice and immersed in 4% PFA for 12 hours before switching to PBS. 300µm-thick coronal sections were cut on a vibratome (Leica VT 1200S). To increase the imaging depth, the sections were cleared following the ScaleSQ protocol (Hama et al., 2015). ScaleS4 buffer was used as a mounting medium (Hama et al., 2015), and spacers were placed on the slides to prevent compressing the sections. Nikon A1R inverted confocal was used to acquire z-stacks that covered the entire extent of the thalamus for each brain, with a 20X objective (NA 0.75 Plan Apo VC). The achieved imaging depth in *z* ranged from 200-250µm. The stacks were imported into Neurolucida software (MBF Bioscience) to trace the migratory morphology of GFP^{+} cells in the dLGN, LP and VP. On average, 2 sections covered the extent of these nuclei in the rostro-caudal dimension and the first time point when GFP^{+} cells were observed there was at E17.5. GFP^{+} cells were not traced in the PO and MG due to their low numbers in these nuclei in the juvenile and adult brains, and the ambiguity in delineating these regions anatomically in the embryonic brains. We did not observe GFP^{+} cells with neuronal morphology in any other TC regions (i.e. outside the FO and HO sensory thalamus) for all ages analysed. In the analysed regions (dLGN, LP, VP), all GFP^{+} somas were annotated using the semi-automated 'Soma' function. The leading processes were traced manually with the 'Tree' function, starting in the middle of the soma and until each process could be unequivocally identified or until the point of bifurcation, for all GFP^{+} cells with a clearly visible and identifiable leading process (44% of

all GFP$^+$ cells at E17.5, 30% at P0.5, 26% at P1.5, 14% at P2.5). The 3D coordinates for each leading process were then exported into Excel, and their orientation was expressed in the brain's coordinate system (x=L-M, y=V-M, z=C-R), as a vector joining the start and end point of the process, using a custom Python script and the Pandas (McKinney, 2010) and Numpy (Walt, Colbert, Varoquaux, 2011) libraries. Each vector was defined by its orientation in spherical coordinates (polar and azimuthal angle), and overall length. Population level orientation data for the dLGN, LP and VP at E17.5 and P0 was plotted as heat-maps, by binning cells according to their spherical coordinates. The bins were then integrated along each axis to reveal a dominant orientation (e.g. for the dLGN, 66% and 69% of cells oriented dorso-ventrally and caudo-rostrally, respectively). Polar histograms of leading process orientation in the dorsal-ventral-lateral-medial plane were also produced.

Spatial clustering analysis

Unsupervised machine learning methods were used to investigate spatial organization of *Sox14*$^+$*Gad1*$^+$ and *Sox14*$^-$*Gad1*$^+$ cells. The 3D models of P14 *Sox14*$^{GFP/+}$ thalamus generated with Neurolucida for NND analysis were again used to obtain the coordinates of all thalamic interneurons.

These data were analysed separately for each brain (n=3) using a custom Python script, and partitioned into clusters using the k-Means algorithm implemented in the library Scikit-Learn (Buitinck et al., 2013). The algorithm takes as input the expected number of clusters *k*.

Multiple values of *k* were tested, and evaluated using the silhouette coefficient metric of clustering performance (Rousseeuw, 1987), also implemented in Scikit-Learn. The silhouette coefficient is equal to the average ratio of distances between points within and between each cluster. More positive scores indicate coherent, well-separated clusters, whereas scores close to zero indicate overlapping clusters. The score was highest (0.472±0.012) for k=2, and the average fraction of all *Sox14*$^+$ and *Sox14*$^-$ cells in each of the resulting clusters was computed across all brains.

We also performed k-Means clustering on the 3D distribution of *Gad1*$^+$ cells obtained from *in situ* hybridisation data from the Allen Mouse Brain Atlas. The silhouette score was again highest (0.512) for k=2, and the resulting clusters have a spatial definition similar to those from the P14 *Sox14*$^{GFP/+}$ thalamus.

Statistics

Comparison of distributions

The Chi-squared test was used to test for significant differences in the thalamus-wide distribution of specific cell classes. This thalamus-wide comparison compensates for

categorical errors arising from a degree of uncertainty in nuclear boundaries, as a result of variation in the sectioning plane and other factors.

For each distribution, average relative cell numbers were computed in Excel. A custom python script was used to compute the Chi-squared statistic, and the corresponding p-value was computed using the Chi-squared cumulative density function implemented in SciPy (Jones et al.).

Change in interneuron numbers in the Sox14 knockout

Unpaired two-sample two-tailed t-test was used, comparing the *Sox14* knockout to *Sox14*$^{GFP/+}$ for each interneuron class separately (n=3 brains/genotype). Total interneuron numbers across all TC nuclei were compared and sampling was consistent between genotypes (each 10th thalamic section was analysed for each brain).

Other statistical analyses used in the study are described in the corresponding sections (Nearest Neighbour Distance calculations and Spatial clustering analysis).

Acknowledgments

We thank the Wohl Cellular Imaging Centre, King's College London for support with imaging and image analysis software. This work was funded by the Biotechnology and Biological Sciences Research Council (BBSRC) grants BB/L020068/1 and BB/R007020/1 to A.D.

Author Contributions

Conceptualization, P.J. and A.D.; Investigation and analysis, P.J., P.C. and X.D.; Resources, T.S. and A.D.; Writing, P.J. and A.D.

Competing Interests

The authors declare no competing interests.

References

Achim, K., Peltopuro, P., Lahti, L., Tsai, H.-H., Zachariah, A., Astrand, M., … Partanen, J. (2013). The role of Tal2 and Tal1 in the differentiation of midbrain GABAergic neuron precursors. *Biology Open*, *2*(10), 990–997. https://doi.org/10.1242/bio.20135041

Achim, K., Salminen, M., & Partanen, J. (2014). Mechanisms regulating GABAergic neuron development. *Cellular and Molecular Life Sciences*, *71*(8), 1395–1415. https://doi.org/10.1007/s00018-013-1501-3

Arcelli, P., Frassoni, C., Regondi, M. C., De Biasi, S., & Spreafico, R. (1997). GABAergic neurons in mammalian thalamus: a marker of thalamic complexity? *Brain Research Bulletin*, *42*(1), 27–37. Retrieved from http://www.ncbi.nlm.nih.gov/pubmed/8978932

Arendt, D., Bertucci, P. Y., Achim, K., & Musser, J. M. (2019). Evolution of neuronal types and families. *Current Opinion in Neurobiology*, *56*, 144–152. https://doi.org/https://doi.org/10.1016/j.conb.2019.01.022

Armstrong, E. (1979). A quantitative comparison of the hominoid thalamus. I. Specific sensory relay nuclei. *American Journal of Physical Anthropology*, *51*(3), 365–381. https://doi.org/10.1002/ajpa.1330510308

Baldwin, M. K. L., Balaram, P., & Kaas, J. H. (2017). The evolution and functions of nuclei of the visual pulvinar in primates. *Journal of Comparative Neurology*, *525*(15), 3207–3226. https://doi.org/10.1002/cne.24272

Bickford, M. E., Wei, H., Eisenback, M. A., Chomsung, R. D., Slusarczyk, A. S., & Dankowsi, A. B. (2008). Synaptic organization of thalamocortical axon collaterals in the perigeniculate nucleus and dorsal lateral geniculate nucleus. *The Journal of Comparative Neurology*, *508*(2), 264–285. https://doi.org/10.1002/cne.21671

Bickford, M. E., Slusarczyk, A., Dilger, E. K., Krahe, T. E., Kucuk, C., & Guido, W. (2010). Synaptic development of the mouse dorsal lateral geniculate nucleus. *Journal of Comparative Neurology*, *518*(5), 622–635. https://doi.org/10.1002/cne.22223

Bolkan, S. S., Stujenske, J. M., Parnaudeau, S., Spellman, T. J., Rauffenbart, C., Abbas, A. I., … Kellendonk, C. (2017). Thalamic projections sustain prefrontal activity during working memory maintenance. *Nature Neuroscience*, *20*, 987. Retrieved from https://doi.org/10.1038/nn.4568

Braak, H., & Bachmann, A. (1985). The percentage of projection neurons and interneurons in the human lateral geniculate nucleus. *Human Neurobiology*, *4*(2), 91–95. http://europepmc.org/abstract/MED/4030427

Buitinck, L., Louppe, G., Blondel, M., Pedregosa, F., Mueller, A., Grisel, O., … Varoquaux, G. (2013). API design for machine learning software: experiences from the scikit-learn project. In *ECML PKDD Workshop: Languages for Data Mining and Machine Learning* (pp. 108–122).

Butler, A. B. (2008). Evolution of the thalamus: a morphological and functional review. *Thalamus & Related Systems*, *4*(1), 35–58. https://doi.org/DOI: 10.1017/S1472928808000356

Cheong, S. K., Tailby, C., Solomon, S. G., & Martin, P. R. (2013). Cortical-Like Receptive Fields in the Lateral Geniculate Nucleus of Marmoset Monkeys. *The Journal of Neuroscience*, *33*(16), 6864 LP – 6876. https://doi.org/10.1523/JNEUROSCI.5208-12.2013

Clascá, F., Rubio-Garrido, P., & Jabaudon, D. (2012). Unveiling the diversity of thalamocortical neuron subtypes. *European Journal of Neuroscience*, *35*(10), 1524–1532. https://doi.org/10.1111/j.1460-9568.2012.08033.x

Clemente-Perez, A., Makinson, S. R., Higashikubo, B., Brovarney, S., Cho, F. S., Urry, A., … Paz, J. T. (2017). Distinct Thalamic Reticular Cell Types Differentially Modulate Normal and Pathological Cortical Rhythms. *Cell Reports*, *19*(10), 2130–2142. https://doi.org/https://doi.org/10.1016/j.celrep.2017.05.044

Crone, S. A., Quinlan, K. A., Zagoraiou, L., Droho, S., Restrepo, C. E., Lundfald, L., … Sharma, K. (2008). Genetic ablation of V2a ipsilateral interneurons disrupts left-right locomotor coordination in mammalian spinal cord. *Neuron*, *60*(1), 70–83. https://doi.org/10.1016/j.neuron.2008.08.009

Delogu, A., Sellers, K., Zagoraiou, L., Bocianowska-Zbrog, A., Mandal, S., Guimera, J., … Lumsden, A. (2012). Subcortical Visual Shell Nuclei Targeted by ipRGCs Develop from a Sox14+-GABAergic Progenitor and Require Sox14 to Regulate Daily Activity Rhythms. *Neuron*, *75*(4), 648–662. https://doi.org/10.1016/j.neuron.2012.06.013

Deneris, E. S., & Hobert, O. (2014). Maintenance of postmitotic neuronal cell identity. *Nature Neuroscience*, *17*(7), 899–907. https://doi.org/10.1038/nn.3731

Eisenstat, D. D., Liu, J. K., Mione, M., Zhong, W., Yu, G., Anderson, S. A., … Rubenstein, J. L. R. (1999). DLX-1, DLX-2, and DLX-5 expression define distinct stages of basal forebrain differentiation. *Journal of Comparative Neurology*, *414*(2), 217–237. https://doi.org/10.1002/(SICI)1096-9861(19991115)414:2<217::AID-CNE6>3.0.CO;2-I

Evangelio, M., García-Amado, M., & Clascá, F. (2018). Thalamocortical Projection Neuron and Interneuron Numbers in the Visual Thalamic Nuclei of the Adult C57BL/6 Mouse .

Frontiers in Neuroanatomy , Vol. 12, p. 27. Retrieved from https://www.frontiersin.org/article/10.3389/fnana.2018.00027

Frangeul, L., Pouchelon, G., Telley, L., Lefort, S., Luscher, C., & Jabaudon, D. (2016). A cross-modal genetic framework for the development and plasticity of sensory pathways. *Nature*, *538*(7623), 96–98. https://doi.org/10.1038/nature19770

Golden, J. A., & Cepko, C. L. (1996). Clones in the chick diencephalon contain multiple cell types and siblings are widely dispersed. *Development*, *122*(1), 65–78. Retrieved from http://www.ncbi.nlm.nih.gov/pubmed/8565854

Golding, B., Pouchelon, G., Bellone, C., Murthy, S., Di Nardo, A. A., Govindan, S., … Jabaudon, D. (2014). Retinal Input Directs the Recruitment of Inhibitory Interneurons into Thalamic Visual Circuits. *Neuron*, *81*(5), 1057–1069. https://doi.org/10.1016/j.neuron.2014.01.032

Granda, R. H., & Crossland, W. J. (1989). GABA-like immunoreactivity of neurons in the chicken diencephalon and mesencephalon. *Journal of Comparative Neurology*, *287*(4), 455–469. https://doi.org/10.1002/cne.902870405

Groh, A., Bokor, H., Mease, R. A., Plattner, V. M., Hangya, B., Stroh, A., … Acsády, L. (2014). Convergence of cortical and sensory driver inputs on single thalamocortical cells. *Cerebral Cortex*, *24*(12), 3167–3179. https://doi.org/10.1093/cercor/bht173

Guillery, R. W. (1995). Anatomical evidence concerning the role of the thalamus in corticocortical communication: a brief review. *Journal of Anatomy*, *187 (Pt 3*(Pt 3), 583–592. Retrieved from https://www.ncbi.nlm.nih.gov/pubmed/8586557

Guillery, R. W., & Sherman, S. M. (2002). Thalamic Relay Functions and Their Role in Corticocortical Communication: Generalizations from the Visual System. *Neuron*, *33*(2), 163–175. https://doi.org/https://doi.org/10.1016/S0896-6273(01)00582-7

Guo, Q., & Li, J. Y. H. (2019). Defining developmental diversification of diencephalon neurons through single-cell gene expression profiling. *Development*, dev.174284. https://doi.org/10.1242/dev.174284

Guo, Z. V, Inagaki, H. K., Daie, K., Druckmann, S., Gerfen, C. R., & Svoboda, K. (2017). Maintenance of persistent activity in a frontal thalamocortical loop. *Nature*, *545*, 181. Retrieved from https://doi.org/10.1038/nature22324

Halassa, M. M., & Kastner, S. (2017). Thalamic functions in distributed cognitive control. *Nature Neuroscience*, *20*(12), 1669–1679. https://doi.org/10.1038/s41593-017-0020-1

Halley, A. C., & Krubitzer, L. (2019). Not all cortical expansions are the same: the coevolution of the neocortex and the dorsal thalamus in mammals. *Current Opinion in Neurobiology*, *56*, 78–86. https://doi.org/https://doi.org/10.1016/j.conb.2018.12.003

Hama, H., Hioki, H., Namiki, K., Hoshida, T., Kurokawa, H., Ishidate, F., … Miyawaki, A. (2015). ScaleS: an optical clearing palette for biological imaging. *Nature Neuroscience*, *18*, 1518. Retrieved from https://doi.org/10.1038/nn.4107

Hayes, S. G., Murray, K. D., & Jones, E. G. (2003). Two epochs in the development of gamma-aminobutyric acidergic neurons in the ferret thalamus. *The Journal of Comparative Neurology*, *463*(1), 45–65. https://doi.org/10.1002/cne.10749

Herkenham, M. (1980). Laminar organization of thalamic projections to the rat neocortex. *Science*, *207*(4430), 532 LP – 535. https://doi.org/10.1126/science.7352263

Hippenmeyer, S., Vrieseling, E., Sigrist, M., Portmann, T., Laengle, C., Ladle, D. R., & Arber, S. (2005). A developmental switch in the response of DRG neurons to ETS transcription factor signaling. *PLoS Biology*, *3*(5), e159–e159. https://doi.org/10.1371/journal.pbio.0030159

Hirsch, J. A., Wang, X., Sommer, F. T., & Martinez, L. M. (2015). How Inhibitory Circuits in the Thalamus Serve Vision. *Annual Review of Neuroscience*, *38*(1), 309–329. https://doi.org/10.1146/annurev-neuro-071013-014229

Hubel, D. H., & Wiesel, T. N. (1962). Receptive fields, binocular interaction and functional architecture in the cat's visual cortex. *The Journal of Physiology*, *160*(1), 106–154. Retrieved from https://www.ncbi.nlm.nih.gov/pubmed/14449617

Hunnicutt, B. J., Long, B. R., Kusefoglu, D., Gertz, K. J., Zhong, H., & Mao, T. (2014). A comprehensive thalamocortical projection map at the mesoscopic level. *Nature Neuroscience*, *17*(9), 1276–1285. https://doi.org/10.1038/nn.3780

Jager, P., Ye, Z., Yu, X., Zagoraiou, L., Prekop, H.-T., Partanen, J., … Delogu, A. (2016). Tectal-derived interneurons contribute to phasic and tonic inhibition in the visual thalamus. *Nature Communications*, *7*, 13579. https://doi.org/10.1038/ncomms13579

Jones, E. (2002). Dichronous appearance and unusual origins of GABA neurons during development of the mammalian thalamus. *Thalamus & Related Systems*, *1*(4), 283–288. https://doi.org/10.1016/S1472-9288(02)00002-X

Jones, E. G. (2007). *The thalamus* (2nd ed.). Retrieved from http://www.cambridge.org/us/academic/subjects/life-sciences/neuroscience/thalamus-2nd-edition?format=WX&isbn=9780521858816#GsbwSMU183VqWWXZ.97

Jones, E., Oliphant, T., Peterson, P., & others. (n.d.). SciPy: Open source scientific tools for Python. Retrieved from http://www.scipy.org/

Kenigfest, N. B., Repérant, J., Rio, J.-P., Belekhova, M. G., Tumanova, N. L., Ward, R., … Ozirskaya, E. V. (1995). Fine structure of the dorsal latreral geniculate nucleus of the turtle, Emys orbicularis: A Golgi, combined hrp tracing and GABA immunocytochemical study. *Journal of Comparative Neurology*, *356*(4), 595–614. https://doi.org/10.1002/cne.903560409

Kenigfest, N. B., Repérant, J., Rio, J.-P., Belekhova, M. G., Ward, R., Vesselkin, N. P., … Herbin, M. (1998). Retinal and cortical afferents to the dorsal lateral geniculate nucleus of the turtle, Emys orbicularis: A combined axonal tracing, glutamate, and GABA immunocytochemical electron microscopic study. *Journal of Comparative Neurology*, *391*(4), 470–490. https://doi.org/10.1002/(SICI)1096-9861(19980222)391:4<470::AID-CNE5>3.0.CO;2-Y

Kimmel, R. A., Turnbull, D. H., Blanquet, V., Wurst, W., Loomis, C. A., & Joyner, A. L. (2000). Two lineage boundaries coordinate vertebrate apical ectodermal ridge formation. *Genes & Development* , *14*(11), 1377–1389. https://doi.org/10.1101/gad.14.11.1377

Lein, E. S., Hawrylycz, M. J., Ao, N., Ayres, M., Bensinger, A., Bernard, A., … Jones, A. R. (2006). Genome-wide atlas of gene expression in the adult mouse brain. *Nature*, *445*, 168. Retrieved from https://doi.org/10.1038/nature05453

Letinić, K., & Kostović, I. (1997). Transient fetal structure, the gangliothalamic body, connects telencephalic germinal zone with all thalamic regions in the developing human brain. *Journal of Comparative Neurology*, *384*(3), 373–395. https://doi.org/10.1002/(SICI)1096-9861(19970804)384:3<373::AID-CNE5>3.0.CO;2-0

Letinic, K., & Rakic, P. (2001). Telencephalic origin of human thalamic GABAergic neurons. *Nature Neuroscience*, *4*(9), 931–936. https://doi.org/10.1038/nn0901-931

Ling, S., Pratte, M. S., & Tong, F. (2015). Attention alters orientation processing in the human lateral geniculate nucleus. *Nature Neuroscience*, *18*(4), 496–498. https://doi.org/10.1038/nn.3967

Marín, O., & Rubenstein, J. L. R. (2001). A long, remarkable journey: Tangential migration in the telencephalon. *Nature Reviews Neuroscience*, *2*(11), 780–790. https://doi.org/10.1038/35097509

Martinez, S., & Alvarado-Mallart, R. M. (1989). Transplanted mesencephalic quail cells colonize selectively all primary visual nuclei of chick diencephalon: a study using heterotopic transplants. *Brain Research. Developmental Brain Research*, *47*(2), 263–274. Retrieved from http://www.ncbi.nlm.nih.gov/pubmed/2519511

Mayer, C., Hafemeister, C., Bandler, R. C., Machold, R., Batista Brito, R., Jaglin, X., … Satija, R. (2018). Developmental diversification of cortical inhibitory interneurons. *Nature*, *555*, 457. Retrieved from https://doi.org/10.1038/nature25999

McKinney, W. (2010). Data Structures for Statistical Computing in Python. In S. van der Walt & J. Millman (Eds.), *Proceedings of the 9th Python in Science Conference* (pp. 51–56).

Métin, C., Alvarez, C., Moudoux, D., Vitalis, T., Pieau, C., & Molnár, Z. (2007). Conserved pattern of tangential neuronal migration during forebrain development. *Development*, *134*(15), 2815 LP – 2827. https://doi.org/10.1242/dev.02869

Mi, D., Li, Z., Lim, L., Li, M., Moissidis, M., Yang, Y., … Marín, O. (2018). Early emergence of cortical interneuron diversity in the mouse embryo. *Science*, *360*(6384), 81 LP – 85. https://doi.org/10.1126/science.aar6821

Miller, J. A., Ding, S.-L., Sunkin, S. M., Smith, K. A., Ng, L., Szafer, A., … Lein, E. S. (2014). Transcriptional landscape of the prenatal human brain. *Nature*, *508*, 199. Retrieved from https://doi.org/10.1038/nature13185

Mo, A., Mukamel, E. A., Davis, F. P., Luo, C., Henry, G. L., Picard, S., … Nathans, J. (2015). Epigenomic Signatures of Neuronal Diversity in the Mammalian Brain. *Neuron*, *86*(6), 1369–1384. https://doi.org/10.1016/j.neuron.2015.05.018

Monory, K., Massa, F., Egertová, M., Eder, M., Blaudzun, H., Westenbroek, R., … Lutz, B. (2006). The endocannabinoid system controls key epileptogenic circuits in the hippocampus. *Neuron*, *51*(4), 455–466. https://doi.org/10.1016/j.neuron.2006.07.006

Montero, V. M. (1987). Ultrastructural identification of synaptic terminals from the axon of type 3 interneurons in the cat lateral geniculate nucleus. *Journal of Comparative Neurology*, *264*(2), 268–283. https://doi.org/10.1002/cne.902640210

Paredes, M. F., James, D., Gil-Perotin, S., Kim, H., Cotter, J. A., Ng, C., … Alvarez-Buylla, A. (2016). Extensive migration of young neurons into the infant human frontal lobe. *Science*, *354*(6308), aaf7073. https://doi.org/10.1126/science.aaf7073

Pasik, P., Pasik, T., & Hámori, J. (1976). Synapses between interneurons in the lateral geniculate nucleus of monkeys. *Experimental Brain Research*, *25*(1), 1–13. Retrieved from http://www.ncbi.nlm.nih.gov/pubmed/817920

Piscopo, D. M., El-Danaf, R. N., Huberman, A. D., & Niell, C. M. (2013). Diverse Visual Features Encoded in Mouse Lateral Geniculate Nucleus. *The Journal of Neuroscience*, *33*(11), 4642 LP – 4656. https://doi.org/10.1523/JNEUROSCI.5187-12.2013

Pouchelon, G., Gambino, F., Bellone, C., Telley, L., Vitali, I., Lüscher, C., … Jabaudon, D. (2014). Modality-specific thalamocortical inputs instruct the identity of postsynaptic L4 neurons. *Nature*, *511*, 471. Retrieved from https://doi.org/10.1038/nature13390

Prekop, H.-T., Kroiss, A., Rook, V., Zagoraiou, L., Jessell, T. M., Fernandes, C., … Wingate, R. J. T. (2018). Sox14 Is Required for a Specific Subset of Cerebello–Olivary Projections. *The Journal of Neuroscience*, *38*(44), 9539 LP – 9550. https://doi.org/10.1523/JNEUROSCI.1456-18.2018

Pritz, M. B., & Stritzel, M. E. (1994). Morphological and GAD immunocytochemical properties of the dorsal lateral geniculate nucleus in a reptile. *Brain Research Bulletin*, *33*(6), 723–726. https://doi.org/https://doi.org/10.1016/0361-9230(94)90239-9

Puelles, L., & Rubenstein, J. L. R. (2003). Forebrain gene expression domains and the evolving prosomeric model. *Trends in Neurosciences*, *26*(9), 469–476. https://doi.org/10.1016/S0166-2236(03)00234-0

Rakić, P., & Sidman, R. L. (1969). Telencephalic origin of pulvinar neurons in the fetal human brain. *Zeitschrift Für Anatomie Und Entwicklungsgeschichte*, *129*(1), 53–82. https://doi.org/10.1007/BF00521955

Rikhye, R. V, Gilra, A., & Halassa, M. M. (2018). Thalamic regulation of switching between cortical representations enables cognitive flexibility. *Nature Neuroscience*, *21*(12), 1753–1763. https://doi.org/10.1038/s41593-018-0269-z

Rikhye, R. V, Wimmer, R. D., & Halassa, M. M. (2018). Toward an Integrative Theory of Thalamic Function. *Annual Review of Neuroscience*, *41*(1), 163–183. https://doi.org/10.1146/annurev-neuro-080317-062144

Rio, J.-P., Reperant, J., Ward, R., Miceli, D., & Medina, M. (1992). Evidence of GABA-immunopositive neurons in the dorsal part of the lateral geniculate nucleus of reptiles: Morphological correlates with interneurons. *Neuroscience*, *47*(2), 395–407. https://doi.org/https://doi.org/10.1016/0306-4522(92)90254-Y

Roth, M. M., Dahmen, J. C., Muir, D. R., Imhof, F., Martini, F. J., & Hofer, S. B. (2015). Thalamic nuclei convey diverse contextual information to layer 1 of visual cortex. *Nature Neuroscience*, *19*(2), 299–307. https://doi.org/10.1038/nn.4197

Rousseeuw, P. J. (1987). Silhouettes: A graphical aid to the interpretation and validation of cluster analysis. *Journal of Computational and Applied Mathematics*, *20*, 53–65. https://doi.org/https://doi.org/10.1016/0377-0427(87)90125-7

Rubio-Garrido, P., Pérez-de-Manzo, F., Porrero, C., Galazo, M. J., & Clascá, F. (2009). Thalamic Input to Distal Apical Dendrites in Neocortical Layer 1 Is Massive and Highly Convergent. *Cerebral Cortex*, *19*(10), 2380–2395. https://doi.org/10.1093/cercor/bhn259

Saalmann, Y. B., & Kastner, S. (2011). Cognitive and Perceptual Functions of the Visual Thalamus. *Neuron*, *71*(2), 209–223. https://doi.org/10.1016/j.neuron.2011.06.027

Saunders, A., Macosko, E. Z., Wysoker, A., Goldman, M., Krienen, F. M., de Rivera, H., … McCarroll, S. A. (2018). Molecular Diversity and Specializations among the Cells of the Adult Mouse Brain. *Cell*, *174*(4), 1015-1030.e16. https://doi.org/https://doi.org/10.1016/j.cell.2018.07.028

Schmitt, L. I., Wimmer, R. D., Nakajima, M., Happ, M., Mofakham, S., & Halassa, M. M. (2017). Thalamic amplification of cortical connectivity sustains attentional control. *Nature*, *545*(7653), 219–223. https://doi.org/10.1038/nature22073

Seabrook, T. A., El-Danaf, R. N., Krahe, T. E., Fox, M. A., & Guido, W. (2013). Retinal Input Regulates the Timing of Corticogeniculate Innervation. *Journal of Neuroscience*, *33*(24), 10085–10097. https://doi.org/10.1523/JNEUROSCI.5271-12.2013

Seabrook, T. A., Krahe, T. E., Govindaiah, G., & Guido, W. (2013). Interneurons in the mouse visual thalamus maintain a high degree of retinal convergence throughout postnatal development. *Neural Development*, *8*(1), 24. https://doi.org/10.1186/1749-8104-8-24

Sgaier, S. K., Lao, Z., Villanueva, M. P., Berenshteyn, F., Stephen, D., Turnbull, R. K., & Joyner, A. L. (2007). Genetic subdivision of the tectum and cerebellum into functionally related regions based on differential sensitivity to engrailed proteins. *Development*, *134*(12), 2325–2335. https://doi.org/10.1242/dev.000620

Shatz, C. J. (1996). Emergence of order in visual system development. *Proceedings of the National Academy of Sciences*, *93*(2), 602 LP – 608. https://doi.org/10.1073/pnas.93.2.602

Sherman, S. M., & Guillery, R. W. (2002). The role of the thalamus in the flow of information to the cortex. *Philosophical Transactions of the Royal Society of London. Series B: Biological Sciences*, *357*(1428), 1695–1708. https://doi.org/10.1098/rstb.2002.1161

Sherman, S. M. (2016). Thalamus plays a central role in ongoing cortical functioning. *Nature Neuroscience*, *16*(4), 533–541. https://doi.org/10.1038/nn.4269

Sherman, S. M. (2004). Interneurons and triadic circuitry of the thalamus. *Trends in Neurosciences*, *27*(11), 670–675. https://doi.org/10.1016/j.tins.2004.08.003

Shi, W., Xianyu, A., Han, Z., Tang, X., Li, Z., Zhong, H., … Shi, S.-H. (2017). Ontogenetic establishment of order-specific nuclear organization in the mammalian thalamus. *Nature Neuroscience*, *20*(4), 516–528. https://doi.org/10.1038/nn.4519

Shimogori, T., Abe, A., Go, Y., Hashikawa, T., Kishi, N., Kikuchi, S. S., … Okano, H. (2018). Digital gene atlas of neonate common marmoset brain. *Neuroscience Research*, *128*, 1–13. https://doi.org/https://doi.org/10.1016/j.neures.2017.10.009

Sousa, V. H., Miyoshi, G., Hjerling-Leffler, J., Karayannis, T., & Fishell, G. (2009). Characterization of Nkx6-2-Derived Neocortical Interneuron Lineages. *Cerebral Cortex*, *19*(suppl_1), i1–i10. https://doi.org/10.1093/cercor/bhp038

Stephan, H., Frahm, H., & Baron, G. (1981). New and Revised Data on Volumes of Brain Structures in Insectivores and Primates. *Folia Primatologica*, *35*(1), 1–29. https://doi.org/10.1159/000155963

Stühmer, T., Puelles, L., Ekker, M., & Rubenstein, J. L. R. (2002). Expression from a Dlx Gene Enhancer Marks Adult Mouse Cortical GABAergic Neurons. *Cerebral Cortex*, *12*(1), 75–85. https://doi.org/10.1093/cercor/12.1.75

Sugahara, F., Murakami, Y., Pascual-Anaya, J., & Kuratani, S. (2017). Reconstructing the ancestral vertebrate brain. *Development, Growth & Differentiation*, *59*(4), 163–174. https://doi.org/10.1111/dgd.12347

Sugahara, F., Pascual-Anaya, J., Oisi, Y., Kuraku, S., Aota, S., Adachi, N., … Kuratani, S. (2016). Evidence from cyclostomes for complex regionalization of the ancestral vertebrate brain. *Nature*, *531*, 97. Retrieved from https://doi.org/10.1038/nature16518

Tasic, B., Menon, V., Nguyen, T. N., Kim, T. K., Jarsky, T., Yao, Z., … Zeng, H. (2016). Adult mouse cortical cell taxonomy revealed by single cell transcriptomics. *Nature Neuroscience*, *19*(2), 335–346. https://doi.org/10.1038/nn.4216

Tasic, B., Yao, Z., Graybuck, L. T., Smith, K. A., Nguyen, T. N., Bertagnolli, D., … Zeng, H. (2018). Shared and distinct transcriptomic cell types across neocortical areas. *Nature*, *563*(7729), 72–78. https://doi.org/10.1038/s41586-018-0654-5

Thompson, A. D., Picard, N., Min, L., Fagiolini, M., & Chen, C. (2016). Cortical Feedback Regulates Feedforward Retinogeniculate Refinement. *Neuron*, *91*(5), 1021–1033. https://doi.org/10.1016/j.neuron.2016.07.040

Tosches, M. A., Yamawaki, T. M., Naumann, R. K., Jacobi, A. A., Tushev, G., & Laurent, G. (2018). Evolution of pallium, hippocampus, and cortical cell types revealed by single-cell transcriptomics in reptiles. *Science*, *360*(6391), 881 LP – 888. https://doi.org/10.1126/science.aar4237

Tremblay, R., Lee, S., & Rudy, B. (2016). GABAergic Interneurons in the Neocortex: From Cellular Properties to Circuits. *Neuron*, *91*(2), 260–292. https://doi.org/10.1016/j.neuron.2016.06.033

Van der Loos, H., & Woolsey, T. A. (1973). Somatosensory Cortex: Structural Alterations following Early Injury to Sense Organs. *Science*, *179*(4071), 395 LP – 398. https://doi.org/10.1126/science.179.4071.395

Veenman, C. L., & Reiner, A. (1994). The distribution of GABA-containing perikarya, fibers, and terminals in the forebrain and midbrain of pigeons, with particular reference to the basal ganglia and its projection targets. *Journal of Comparative Neurology*, *339*(2), 209–250. https://doi.org/10.1002/cne.903390205

Walt, S. van der, Colbert, S. C., & Varoquaux, G. (2011). The NumPy Array: A Structure for Efficient Numerical Computation. *Computing in Science & Engineering*, *13*(2), 22–30. https://doi.org/10.1109/MCSE.2011.37

Wang, S., Eisenback, M. A., & Bickford, M. E. (2002). Relative distribution of synapses in the pulvinar nucleus of the cat: Implications regarding the “driver/modulator” theory of thalamic function. *Journal of Comparative Neurology*, *454*(4), 482–494. https://doi.org/10.1002/cne.10453

Wong, S. Z. H., Scott, E. P., Mu, W., Guo, X., Borgenheimer, E., Freeman, M., … Nakagawa, Y. (2018). In vivo clonal analysis reveals spatiotemporal regulation of thalamic nucleogenesis. *PLOS Biology*, *16*(4), e2005211. Retrieved from https://doi.org/10.1371/journal.pbio.2005211

Zeater, N., Cheong, S. K., Solomon, S. G., Dreher, B., & Martin, P. R. (2015). Binocular Visual Responses in the Primate Lateral Geniculate Nucleus. *Current Biology*, *25*(24), 3190–3195. https://doi.org/10.1016/j.cub.2015.10.033

Supplementary Figures

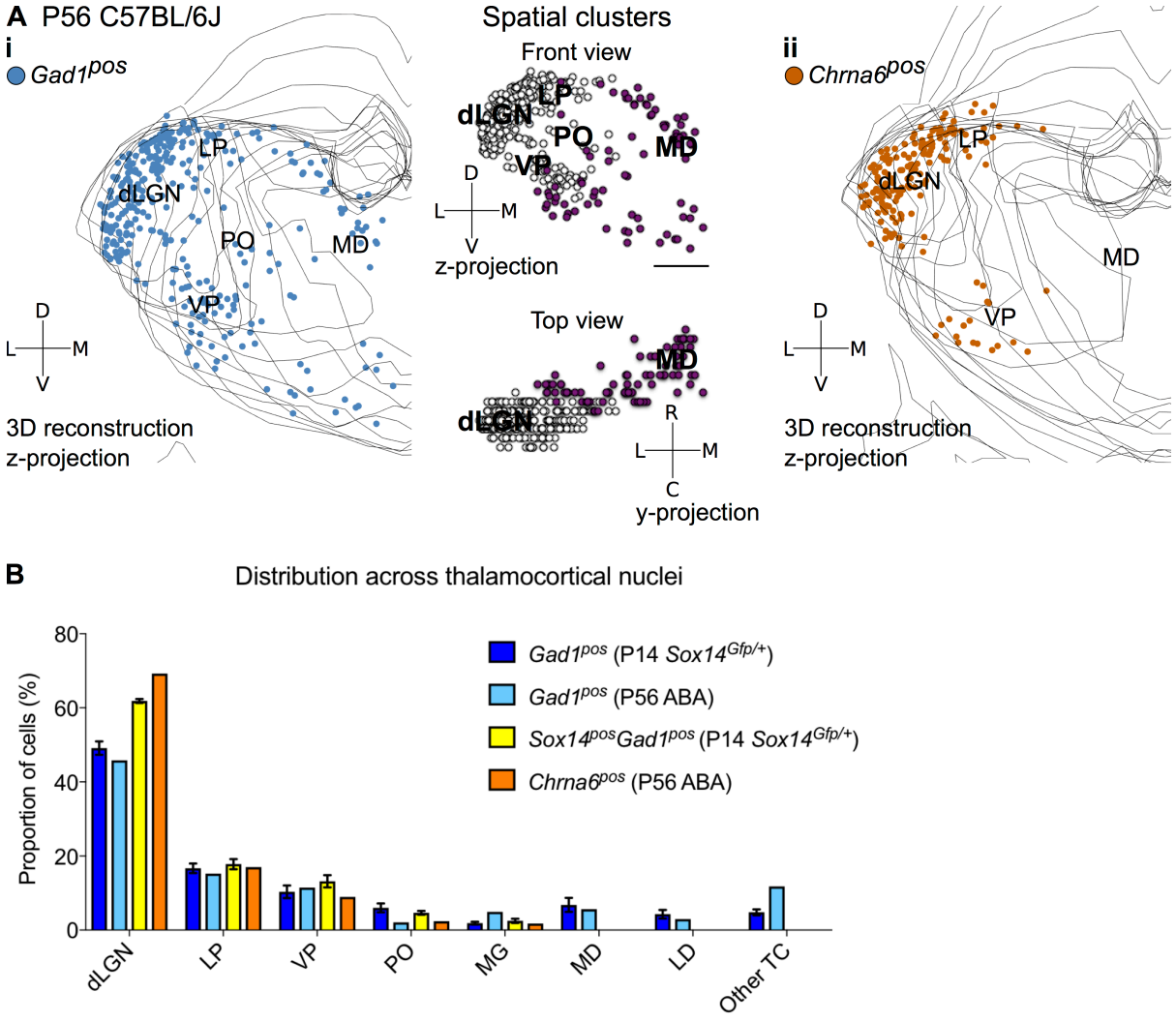

Supplementary Figure 1. A. 3D reconstruction of a representative P56 mouse thalamus from tracing every eight 25µm-thick coronal section, displayed as a z-projection and showing distribution of (i) *Gad1*$^{+}$ and (ii) *Chrna6*$^{+}$ cells. In (i), k-Means clustering was applied to the data using k=2 (highest silhouette score, 0.512); the resulting spatial clusters are shown as a z- and y-projection and colour-coded. One dot represents one neuron. ISH data was downloaded from the Allen Mouse Brain Atlas (© 2004 Allen Institute for Brain Science. Allen Mouse Brain Atlas. Available from: mouse.brain-map.org; Lein et al., 2006). **B.** Distribution of *Gad1*$^{+}$ and *Chrna6*$^{+}$ cells across TC nuclei (n=1 brain/marker) is compared to all *Gad1*$^{+}$ and *Sox14*$^{+}$*Gad1*$^{+}$ cells from P14 *Sox14*$^{GFP/+}$ thalamus (n=3 brains; see also Fig. 1).

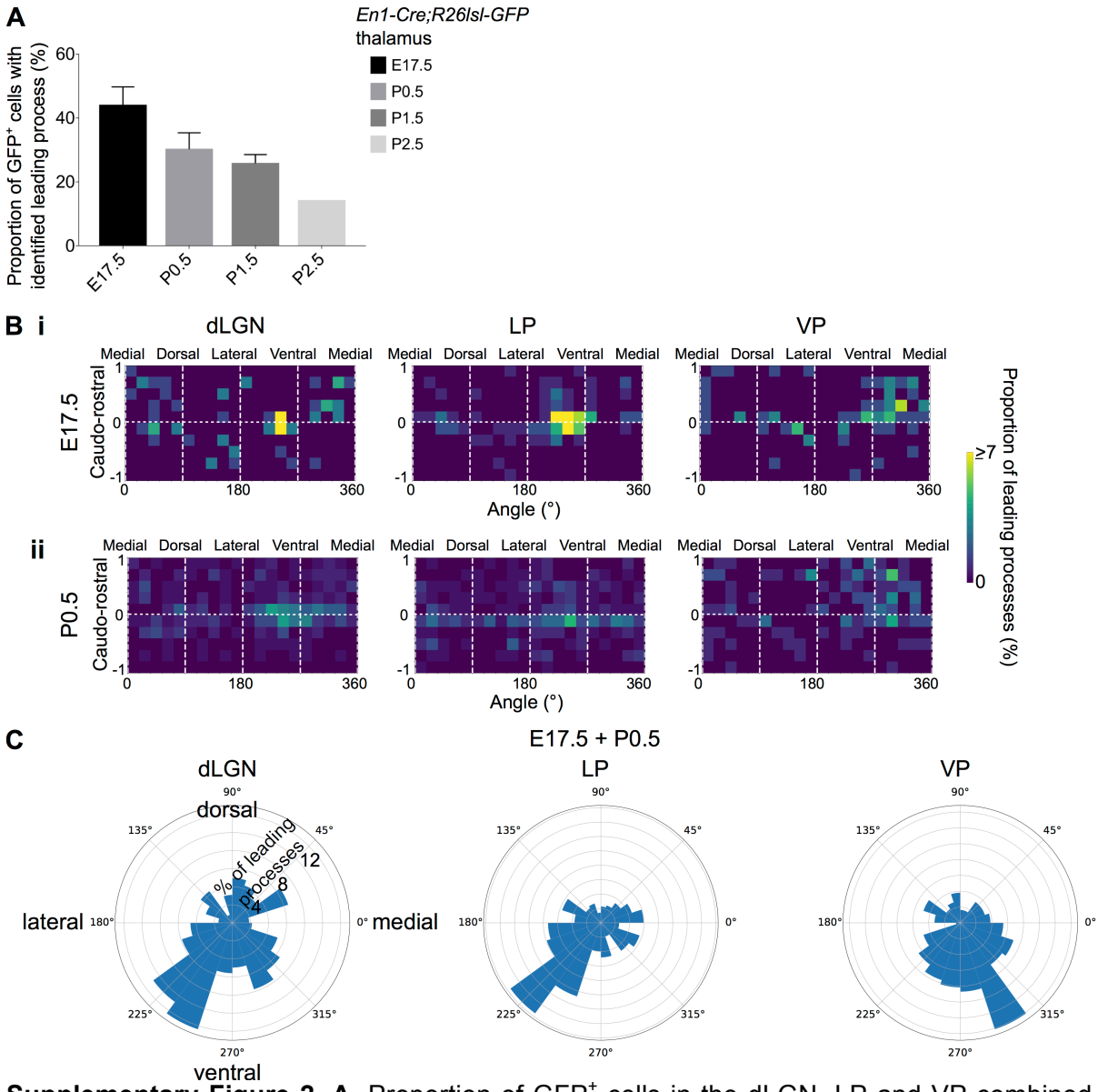

Supplementary Figure 2. A. Proportion of GFP$^+$ cells in the dLGN, LP and VP combined, for which a leading process could be identified, in E17.5-P2.5 *En1-Cre;R26lsl-GFP* brains (mean±SE, n=3 brains/developmental stage, apart from P2.5 where n=1 brain). **B.** Frequency distribution of leading process orientation for GFP$^+$ cells in the dLGN, LP and VP at (i) E17.5 and (ii) P0.5 separately, represented in heat maps (n=3 brains/developmental stage). **C.** Polar histograms of leading process orientation in the latero-medial and ventro-dorsal plane for GFP$^+$ cells in the dLGN, LP and VP at E17.5 and P0 combined (n=3 brains/developmental stage).

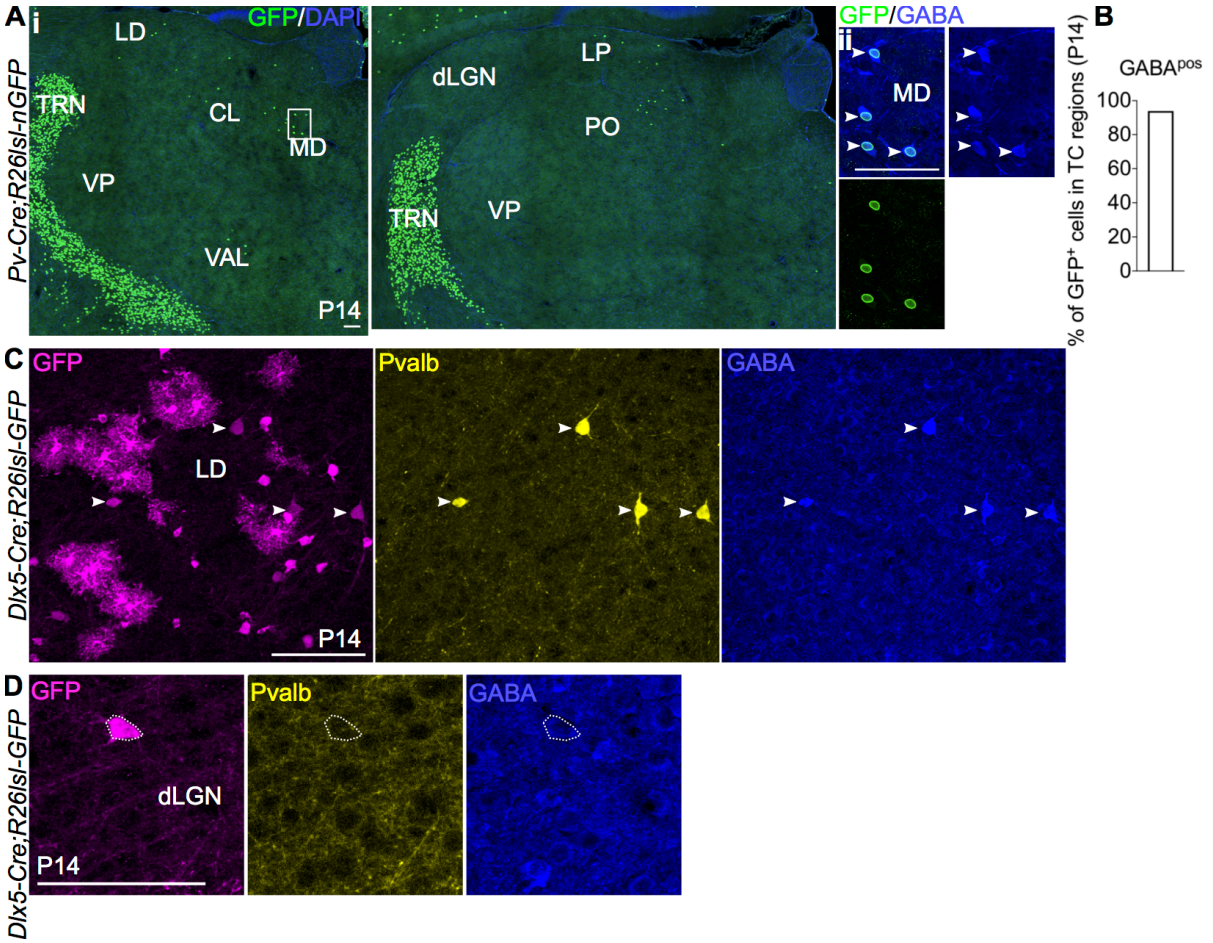

Supplementary Figure 3. A. (i) Representative coronal sections of P14 *Pv-Cre;R26lsl-nGFP* thalamus with GFP$^+$ cells present in the MD, LD, CL, VAL, LP and PO (considering TC regions only). Scale bar, 100µm. (ii) GFP$^+$ cells in TC regions express GABA at P14. Scale bar, 100µm. **B.** Proportion of GFP$^+$ cells in TC regions co-expressing GABA at P14 (mean, n=2 brains). **C.** Clusters of Pvalb$^-$GABA$^-$*Dlx5*$^+$ glia-like cells are observed across TC regions in the *Dlx5-Cre;R26lsl-GFP* line at P14, as shown for the LD. White arrows mark Pvalb$^+$GABA$^+$*Dlx5*$^+$ cells. Scale bar, 100µm. **D.** Pvalb$^-$*Dlx5*$^+$ cells with neuronal morphology do not express GABA. Scale bar, 100µm.

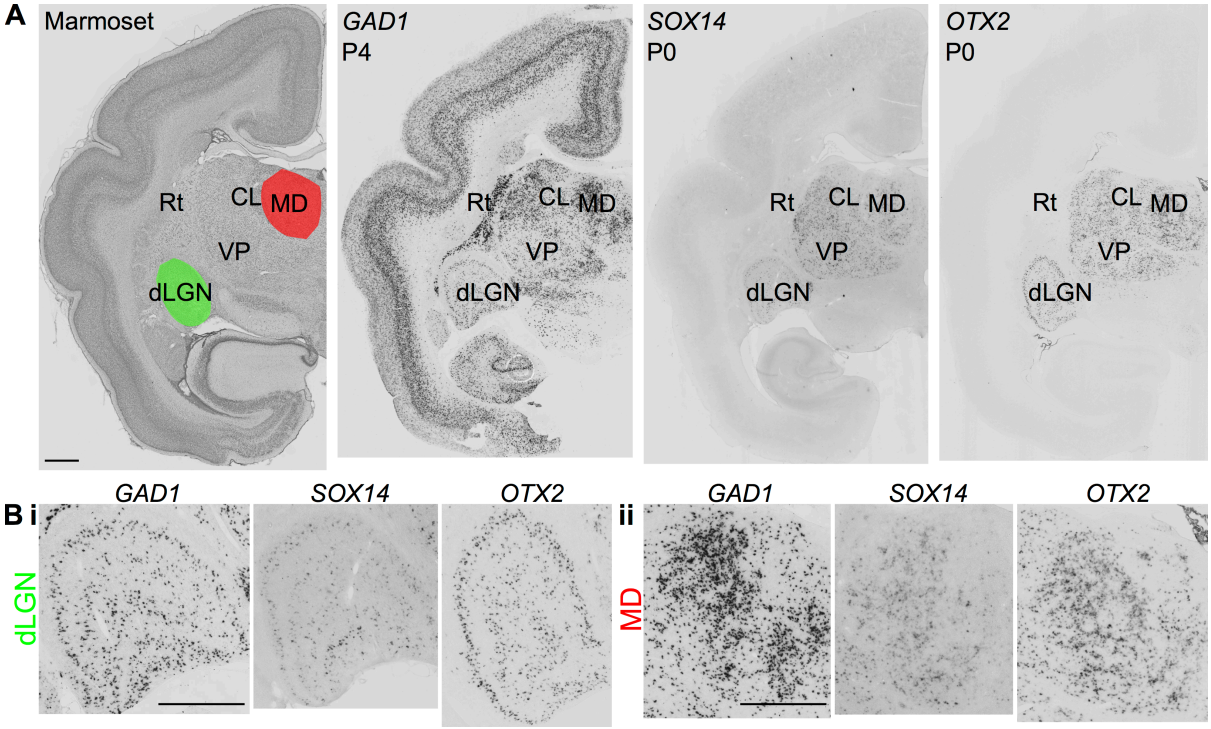

Supplementary Figure 4. A. Representative coronal sections of P0-4 marmoset thalamus showing *GAD1*, *SOX14* and *OTX2* expression. Scale bar, 1000μm. **B.** Expression of *GAD1*, *SOX14* and *OTX2* in the marmoset (i) dLGN and (ii) MD. Scale bar, 1000μm. Source of ISH: the Marmoset Gene Atlas (Available from: https://gene-atlas.brainminds.riken.jp).